UNIVERSIDADE FEDERAL DO RIO GRANDE DO SUL
FACULDADE DE ODONTOLOGIA
PROGRAMA DE PÓS-GRADUAÇÃO EM ODONTOLOGIA
ÁREA DE CONCENTRAÇÃO CLÍNICA ODONTOLÓGICA –
MATERIAIS DENTÁRIOS

DESENVOLVIMENTO E CARACTERIZAÇÃO DE UM CIMENTO DE α-TRICÁLCIO FOSFATO E SULFATO DE CÁLCIO EM FORMA DE ESPUMA PARA REGENERAÇÃO ÓSSEA

ANDREA SCHAEFFER

Porto Alegre
2022

ANDREA SCHAEFFER

DESENVOLVIMENTO E CARACTERIZAÇÃO DE UM CIMENTO DE α-TRICÁLCIO FOSFATO E SULFATO DE CÁLCIO EM FORMA DE ESPUMA PARA REGENERAÇÃO ÓSSEA

Tese apresentada como requisito obrigatório à obtenção do título de doutora em Odontologia da Faculdade de Odontologia na área de concentração em Clínica Odontológica – Materiais Dentários da Universidade Federal do Rio Grande do Sul.

Orientadora: Profa. Dra. Susana Maria Werner Samuel

Porto Alegre
2022

DEDICATÓRIA

Dedico ao meu pai, Lirio Schaeffer, que me impulsionou e incentivou, desde minha graduação, a embarcar no mundo da pesquisa.

AGRADECIMENTOS

Ao **Giovanni Aimi,** meu marido, pelo apoio fundamental, compreensão e muita paciência. Obrigada pelo carinho, amor e dedicação ao Giorgio na minha ausência.

Aos **meus pais, Eliane e Lírio,** aos sogros**, Alcides e Edith** e padrinhos **Cleusa e Mauro,** por terem dado todo apoio possível cuidando com amor e carinho do amado neto Giorgio.

Ao **professor Luis Alberto dos Santos,** minha referência em biomateriais para realizar este trabalho. Muito obrigada por ser esse grande incentivador e pelo fornecimento do material para que a pesquisa fosse realizada.

À **professora Susana Maria Werner Samuel,** minha orientadora que participa há mais de 20 anos na minha vida acadêmica, agradeço a oportunidade e confiança.

Ao **professor Fabrício Mezzomo Collares** que viabilizou essa pesquisa dentro do LAMAD da UFRGS.

Às colegas **Gabriela Balbinot** e **Isadora Martini Garcia**, obrigada pela ajuda dedicada junto ao LAMAD e por dividir comigo seus conhecimentos e experiências.

À **professora Lina** e ao **Douglas** pelo acesso ao LABIM da UFRGS.

Ao **professor Fabrício Faina** do Instituto de Física pela ajuda na realização dos ensaios no Instituto de Física e Geologia da UFRGS.

À **Júlia Cassel,** muito obrigada pela ajuda na reta final do trabalho.

Ao **Programa de Pós-Graduação em Odontologia** pela oportunidade de realizar o Doutorado.

Aos meus pacientes, por terem participado indiretamente deste processo apoiando, torcendo e entendendo minha ausência no consultório.

“Todo grande progresso da ciência resultou de uma nova audácia da imaginação”

John Dewey

RESUMO

Cimentos de fosfato de cálcio (CPCs) são amplamente estudados como alternativa de biomaterial preenchedor não estrutural em cirurgias maxilofaciais, neurológicas e ortopédicas. A possibilidade de ser injetável permite reparar defeitos ósseos pequenos e irregulares com acesso minimamente invasivo e reduzir o tempo cirúrgico. O cimento deve degradar-se em um ritmo adequado para permitir neoformação óssea simultaneamente. A taxa de degradação depende de propriedades como a razão molar entre cálcio/fosfato (Ca/P), estrutura cristalina, área de superfície, porosidade e tamanho de poros. Uma via suficientemente porosa, com poros interligados, é necessária para permitir a formação de vasos sanguíneos e proliferação de células osteoprogenitoras. O objetivo deste estudo foi desenvolver e caracterizar um cimento preparado em forma de espuma, constituído pela fase alfa do fosfato tricálcico (α-TCP) e sulfato de cálcio hemidratado (CSH). As proporções entre α-TCP/CSH foram: 90/10 (G90), 80/20 (G80), 70/30 (G70) respectivamente. A fase líquida foi composta por hidrogeno fosfato dissódio, surfactante, alginato de sódio e água destilada. Um grupo permaneceu sem CSH para ser usado como controle. A espuma foi obtida com a utlização de seringas unidas por um conector de PVC, de forma que a fase líquida e o ar foram misturados rapidamente empurrando os dois êmbolos das seringas alternadamente em direções opostas. Posteriormente, o volume de espuma foi bombeado para outra seringa contendo α-TCP e pó de CSH até a formação de um cimento espumoso homogêneo. As características avaliadas foram: distribuição do tamanho dos poros, percentual de porosidade, estrutura cristalográfica e morfologia, bioatividade, degradação e pH. A Microtomografia computadorizada (micro-CT) revelou uma distribuição aleatória e grande variação de tamanho de poros (10μm a 1mm). A caracterização pela difração de RX (DRX) apresentou aumento dos picos de hidroxiapatita deficiente em cálcio (CDHA) em todos os grupos após a completa reação de hidrólise do α-TCP e CSH após imersão em SBF. As análises pelo microscópio eletrônico de varredura (MEV) confirmaram os resultados do DRX e da espectroscopia no infravermelho por transformada de Fourier (FTIR) mostrando a variação superficial entre os grupos nos diferentes tempos de imersão. G90 e G80 exibiram formas petalóides de CDHA mais definidas após imersão na solução que simula fluido corpóreo (SBF). Os cimentos bifásicos (α-TCP/CSH) preparados em forma de espuma apresentaram maior porcentagem de poros ($p<0,05$) do que o grupo do α-TCP sem CSH. Os grupos com CSH apresentaram características desejáveis e promissoras para utilização em regeneração óssea. Estudos de biocompatibilidade e “in vivo” são necessários para confirmação destes achados.

Palavras-chave: cimento injetável, cimento em espuma, fosfato de cálcio, sulfato de cálcio, porosidade, bioatividade, SBF

ABSTRACT

Calcium phosphate cement (CPC) has been widely studied as a synthetic biomaterial alternative for bone regeneration. Injectability allows to repair small and irregular defects with minimally invasive access and reduce surgical time. CPC should degrade at an appropriate rate to allow bone neoformation simultaneously. The degradation rate depends on the properties of CPC such as molar ratio calcium/phosphate (Ca/P), crystalline structure, surface area, porosity, and pore size. A sufficiently porous pathway, with interconnected pores, is necessary to allow the formation of blood vessels and proliferation of osteoprogenitor cells. The aim of this study was to prepare and characterize a foamed cement consisting of the alpha phase of tricalcium phosphate (α-TCP) and hemidratated calcium sulfate (CaSO4 1/2H2O; CSH). The proportions between α-TCP/CSH wt% were: 90/10 (G90), 80/20 (G80), 70/30 (G70) respectively. The foamed liquid phase was composed of sodium hydrogen phosphate, a surfactant, sodium alginate and distilled water. One group remained without CSH to be used as control. The foam was obtained using syringes joined by a PVC connector, so that the liquid phase and air were quickly mixed by pushing the two plungers of the syringes alternately in opposite directions. Subsequently, the foam volume was pumped into another syringe containing α-TCP and CSH powder until a homogeneous foamed cement was formed. The characteristics evaluated were pore size distribution, porosity percentage, crystallographic and morphology structure, bioactivity, and pH. X-ray computed microtomography (micro-CT) images of all samples revealed a random distribution and wide size variation of pores ranging from 10μm to 1mm. X-ray diffraction (XRD) analysis showed calcium deficient hydroxyapatite (CDHA) peaks increased in all groups with completed hydrolyses reaction of α-TCP and CSH. Observations by SEM confirmed the XRD and Fourier- transformed infrared (FTIR) results and showed a superficial variation between the groups at different immersion times. G90 and G80 exhibited more defined petaloid forms of CDHA after immersion in a solution that simulates body fluid (SBF). Biphasic cements (α-TCP/CSH) showed higher percentage of pore ($p<0.05$) than the α-TCP group without CSH. The foamed cements groups consisting of α-TCP and CSH showed desirable and promising characteristics for bone regeneration. Biocompatibility and “in vivo” studies are needed to confirm these findings.

Keywords : Injectable cement; foamed cement, calcium phosphate; calcium sulfate; porosity; bioactivity, SBF.

Sumário

1 INTRODUÇÃO

Atualmente, é expressiva a demanda de pesquisas por biomateriais que promovam o reparo ou substituição de tecidos ósseos perdidos pelo envelhecimento e/ou razões patológicas. Com o aumento da expectativa de vida, o avanço no desenvolvimento de tecnologias dentro da ciência dos biomateriais é fundamental (MONTOYA et al., 2021).

Diferentes tratamentos regenerativos ósseos são aplicados e a escolha adequada é muito importante para o sucesso clínico. A mistura de osso autógeno e substitutos ósseos de origem xenógena ou biomateriais sintéticos são composições mais comumente utilizadas (RAGHOEBAR et al., 2019).

O tecido ósseo autógeno é considerado padrão ouro principalmente por atender os critérios de osteocondução, osteoindução e osteogênese (LEGEROS, 2002). A propriedade de osteocondução se deve ao fato de o enxerto possuir uma matriz que serve de arcabouço para deposição e reabsorção óssea e promover a quimiotaxia e migração de células progenitoras que se diferenciarão em osteogênicas (SAKKAS et al., 2017). A medida que o osso autógeno é reabsorvido, são liberados fatores de crescimento (proteínas ósseas morfogenéticas), células perivasculares migram dos vasos sanguíneos neoformados (angiogênese) e se diferenciam em osteoblastos, caracterizando a osteoindução. Por último, a capacidade do enxerto autógeno de levar células como os osteócitos e células progenitoras ou osteoblastos já diferenciados, capazes de produzir matriz óssea ao leito receptor, caracteriza a osteogênese (BUSER, 2010; HANDA, 2012).

Por outro lado, o enxerto autógeno tem uma grande desvantagem, a necessidade de uma cirurgia adicional na área doadora. Além da quantidade limitada de tecido, discrepância anatômica entre área doadora e receptora, aumento de 20 a 30% na morbidade, maior período de convalescença e o risco de contaminação na região doadora, limitam a indicação e aceitação pelos pacientes do enxerto autógeno (AGHDASI, 2012; LI et al., 2017).

Alternativas como enxerto homólogo, obtido de indivíduo da mesma espécie; heterólogo, proveniente de indivíduo de diferentes espécies; também apresentam limitações específicas (HAUGEN et al., 2019). Desta forma, biomateriais sintéticos destacam-se como substitutos ósseos por não provocarem desordens funcionais e pela grande disponibilidade (TAO et al., 2018).

Segundo Habraken et al. (2007), descreveram as características de um biomaterial ideal para uso na engenharia de tecidos ósseos:

- biodegradável para permitir a remodelação óssea
- macroporoso para permitir o crescimento tecidual;
- mecanicamente estável e fácil de manusear;
- osteocondutivo para orientar o crescimento ósseo ao redor e dentro do material;
- adequado para funcionar como um portador para fatores de crescimento ou células.

Diversos são os estudos com biomateriais sintéticos em busca de uma estrutura biomimética que corresponda aos requisitos biológicos, físico-químicos, mecânicos e metabólicos específicos de cada parte do corpo humano (FERNANDEZ-YAGUE et al., 2015; TOVANI et al, 2020).

1.1 FOSFATO DE CÁLCIO

Entre estes biomateriais que se destinam à regeneração óssea,encontra-se o fosfato de cálcio (CaP), amplamente utilizado como substituto ósseo desde a década de 1920 e considerado padrão ouro devido a sua biocompatibilidade, osteocondutividade e semelhança com a fase mineral do tecido ósseo. A composição química dos CaPs conta com múltiplos íons, incluindo o cálcio (Ca^{2+}), ortofosfato (PO_4^{3-}), metafosfato (PO^{3-}), pirofosfato ($P_2O_7^{4-}$), hidrogênio (H^+) ou hidróxido (OH^-) (ELIAZ et al., 2017; KUCKO et al., 2019). A tabela 1 apresenta as características de alguns compostos de fosfato de cálcio.

Tabela 1. Alguns compostos de fosfato de cálcio.

Nome	Sigla	Fórmula química	Ca/P	Solubilidade em água a 25℃, mg/L
Hidroxiapatita	HA	$Ca_{10}(PO_4)_6(OH)_2$	1,67	~0,0003
Hidroxiapatita deficiente em cálcio	CDHA	$Ca_{10-x}(HPO_4 \text{ or } CO_3)_x(PO_4)_{6-x}(OH \text{ ou } ½\ CO_3)_{2-x}$ (0<x<1)	1,5 – 1,67	~0,0094
Fosfato dicálcio dihidratado (brushita)	DCPD	$CaHPO_4.2H_2O$	1	~0,088
α-Fosfato tricálcico	α-TCP	$\alpha\text{-}Ca_3(PO_4)_2$	1,5	~0,00025
β-Fosfato tricálcico	β-TCP	$\beta\text{-}\ Ca_3(PO_4)_2$	1,5	~0,0005

Fonte: Adaptado de Dorozhkin (2013).

Entre os fosfatos de cálcio mais difundidos, destacam-se a hidroxiapatita (HA) ($Ca_{10}(PO_4)_6(OH)_2$), fosfato de β tricálcico (β-TCP) e fosfato de α tricálcico (α-TCP). A HA é particularmente promissora para a regeneração devido à sua composição e estrutura semelhante a fase mineral dos tecidos ósseos. Nas últimas décadas, a síntese de HA tem sido investigada para diferentes aplicações, incluindo *scaffolds* (arcabouços), blocos, grânulos, pós, pastas/cimentos injetáveis, revestimentos para implantes. A HA estequiométrica apresenta alta estabilidade em pH fisiológico, limitando sua reabsorção a longo prazo. (GINEBRA et al., 2018; GRAZIANI et al., 2018; USKOKOVIC et al., 2020)

As formas alotrópicas β e α-TCP exibem composição química semelhante, porém diferentes estruturas cristalinas, densidade e solubilidade, resultando em diferentes desempenhos biológicos. Segundo Liu (2015), possuem superfícies que facilitam a adsorção de proteínas com potencial elevado de osteoindução. A fase β-TCP é mais estável a temperatura ambiente enquanto a fase α-TCP é a mais solúvel. Bohner (2000) afirmou ter maior bioatividade possibilitando absorção de uma maior quantidade de íons Ca^{2+} e PO_4^{3-} e substituição por novo tecido ósseo. Jeong et al. (2019) enfatizou que o notável interesse no α-TCP vem da combinação de sua solubilidade e baixa relação Ca/P. O α-TCP tem maior energia específica e pode ser misturado a outros fosfatos de cálcio e hidrolisado (DOROZHKIN, 2009).

O processo de hidratação do sal de α-TCP foi descrito pela primeira vez por Monma e Kanazawa (1976). As equações (1 e 2) descrevem a hidrólise do α-TCP e a obtenção de hidroxiapatita deficiente em cálcio (CDHA). A cinética desta

reação ocorre lentamente à temperatura fisiológica e pode ser favorecida variando o tamanho de partícula do pó, alterarando a relação líquido/pó (mL/g) e modificando a composição química da fase líquida. Diferentes aditivos podem ser usados, como por exemplo ortofosfatos solúveis: ácido fosfórico, fosfato monocálcico mono-hidratado (MCPM – $Ca(H_2PO_4)_2•H_20$), fosfato monossódico (NaH_2PO_4) entre outros), os quais promovem a dissolução pela acidificação do pH do sistema (DOROZHKIN, 2009).

A reação ocorre através da dissolução dos íons Ca^{2+} e PO_4^{3-} na fase líquida conforme a equação:

$$3Ca_3(PO_4)2 + H_2O \rightarrow 9Ca_2+ + 6PO_4\,^{3-} + H_2O. \quad (1)$$

Posteriormente, a solução torna-se supersaturada com apatita, levando à formação de uma rede emaranhada de cristais de CDHA:

$$9Ca_2+ + 6PO_4^{3-} + H_2O \rightarrow Ca_9HPO_4(PO_4)_5(OH). \quad (2)$$

Essas reações são conhecidas como reações de dissolução-precipitação. (GINEBRA et al., 2004) Devido à sua alta solubilidade, o α-TCP tem sido usado para a preparação de CaP arcabouços bifásicos, capazes de conjugar as propriedades osteogênicas da HA e o comportamento de reabsorção do TCP (LOBO et al., 2010; MAJI et al., 2020).

1.2 CIMENTOS DE CaP À BASE DE α-TCP

Substitutos ósseos à base de CaP estão disponíveis como grânulos, blocos e cimentos. Legeros (1982), Brow e Chow (1983) foram os precursores dos estudos de cimentos ósseos a base fosfato de cálcio (CPC). São biocompatíveis, não provocam resposta inflamatória nem geram calor (SCHRÖTER et al., 2020). Apresentam propriedades biológicas como bioatividade, bioreabsorbabilidade e osteocondutividade, possuem comportamento com potencial osteoindutivo, endurecem em condições fisiológicas a 37ºC e oferecem uma característica única de serem moldáveis e injetáveis, permitindo preenchimento, minimamente invasivo, de defeitos ósseos irregulares (TORRECILLA et al., 2021).

Além de possuir as propriedades biológicas dos CPC, o cimento baseado na fase α do fosfato de cálcio, quando hidratado, reage formando uma rede de cristais microagulhados ou em forma de pétalas de CDHA entrelaçados, proporcionando assim uma rigidez mecânica (BOHNER, 2010; O'NEIL et al., 2017). Canal et al. (2011) e Santos (2003) relatam que a resistência à compressão, no melhor dos casos, consegue igualar-se à do osso trabecular, o que limita sua aplicação a áreas com carga moderada ou sem carga (LIU et al., 2013). Como exemplos de aplicação, pode-se citar o levantamento de seio maxilar com implante imediato, regeneração de defeitos periodontais de 2 ou 3 paredes remanescentes, defeitos após remoção de cistos, após apicetomias, após remoção de dentes impactados, expansão cirúrgica de rebordo alveolar, também conhecida como *Split Crest*, recobrimento de fenestrações ósseas durante a instalação de implantes e preenchimentos de *gaps,* lacuna entre rebordo alveolar e implante instalado imediamente após a extração.

Apesar da semelhança na composição química e estrutural da CDHA, o cimento de α-TCP tem a desvantagem de ser muito estável *in vivo,* relativamente insolúveis em pH neutro a ponto de levar de 1 a 2 anos para ser reabsorvido (HANKERMEYER et al., 2002). A taxa de reabsorção depende de alguns fatores, como por exemplo, o pH. A solubilidade aumenta com pH mais ácido de modo que podem ser reabsorvidos por osteoclastos durante a remodelação óssea. Outros fatores como a porosidade, tamanho dos poros, cristalinidade, pureza química e rugosidade superficial do biomaterial, ambiente e temperatura, também interferem na taxa de reabsorção (ALVES, 2005; HOPPE, 2011).

1.3 DEGRADAÇÃO (DISSOLUÇÃO E REABSORÇÃO)

No tratamento de defeitos ósseos, materiais reabsorvíveis são desenvolvidos para se degradarem progressivamente fornecendo ao longo do tempo uma via para neoformação óssea e assim propiciar que células e fatores de crescimento desempenhem seu papel fisiológico (LU et al.,2018; Wei et al. 2020). Idealmente, a taxa de degradação dos CPCs deve ser semelhante à taxa de neoformação óssea para fornecer suporte mecânico onde baixas ou nenhuma carga são aplicadas e aporte sanguíneo adequado. Degradação muito lenta ou muito rápida impede esse processo. (BOHNER, 2010; GINEBRA et al., 2010; HABRAKEN et al., 2016).

O controle da degradação do CPC baseados em α-TCP pode ser descrito como a combinação de dois mecanismos diferentes: dissolução passiva e reabsorção ativa. A degradação ou dissolução passiva no líquido extracelular quando *in vivo* ou em uma solução *in vitro,* depende da espessura da camada de apatita formada na superfície dos grãos, cristalinidade, razão Ca/P e pH local. A degradação ou reabsorção ativa ocorre através da atividade celular (osteoclastos, células gigantes, macrófagos e mediadores químicos que causam a redução do pH (LEGEROS, 2002).

Inicialmente, a reação é controlada pela área superficial dos grãos de α-TCP em contato com a solução (dissolução), formando uma camada fina e permeável ao transporte iônico ao redor das partículas. O processo continua até que toda superfície dos grãos esteja coberta por uma camada de apatita de espessura suficientemente grande para que o processo de difusão passe a ser mais lento que a taxa de dissolução do α-TCP. Estudos *in vivo* revelaram que quanto maior a área superficial, maior o contato com fluidos corpóreos, maior a taxa de degradação das partículas (GINEBRA et al., 2004; CAMIRÉ et al., 2005; BOHNER et al., 2006; ŞAHIN, 2018; MONTOYA et al, 2021).

A degradação das partículas de α-TCP na fase líquida do cimento marca o início da reação de presa. A fase liquida passa a receber íons de Ca e P até se tornar sobressaturada, precipitando assim a fase mais estável, CDHA, sobre a superfície das partículas de α-TCP, por ser o local de maior concentração de íons e o de menor energia superficial. As partículas de α-TCP continuam a solubilizar, atravessando a barreira de CDHA que se torna mais espessa à medida que a reação de presa evolui (GINEBRA, 1997). No final da reação, quando praticamente todo α-TCP foi consumido, haverá uma casca de CDHA com um vazio em seu interior (grãos de Hadley), local onde originalmente se encontrava a partícula de α-TCP totalmente solubilizada. (HADLEY et al., 2000).

Após a presa, os cristais em forma de agulhas ou pétalas precipitam e crescem epitaxialmente, sendo os responsáveis pela aderência e entrecruzamento dos grãos. Com o tempo, a microestrutura muda o formato para hastes, como resultado da maior cristalinidade e uma maior quantidade de cristais preenchendo os vazios que podem ser altamente compactos em algumas áreas de alta densidade e mais separados em áreas com maior porosidade (AMBARD and MEUNINGHOFF, 2006)

1.4 ABORDAGENS PARA AUMENTAR A TAXA DE DEGRADAÇÃO

Dorozhkin (2007) destaca os requisitos aos quais um material ideal para regeneração óssea deve atender como possuir uma taxa de reabsorção comparável com a formação de novo tecido ósseo, porosidade igual ou maior a 100μm e estabilidade mecânica suficiente. Assim, graças à versatilidade dos fosfatos de cálcio, diferentes tipos de processamento podem ser utilizados a fim de se obter diversas combinações de morfologias, propriedades e composições químicas, dependendo do tipo de aplicação.

A modificação da composição química dos CPC pode incluir todos compostos iônicos de minerais presentes no corpo humano como Na^{+}, K^{+}, Mg^{2+}, Ca^{2+}, H^{+}, Sr^{2+}, Si^{4+}, Fe^{2+} e ânions: PO_4^{3-}, HPO_4^{2-}, $H_2PO_4^{-}$, CO_3^{2-}, HCO_3^{-}, SO_4^{2-}, HSO_4^{-}, Cl^{-}, F^{-}, SiO_4^{4-}. Portanto, cimentos constituídos por CaP e outros sais de cálcio como sulfato de cálcio (CS), pirofosfato de cálcio, hidróxido de cálcio, silicato de cálcio e fosfato de estrôncio são possíveis abordagens para o aumento da taxa de degradação (DOROZHKIN, 2018).

Alterar a razão líquido/pó (L/P) é outra abordagem que determina, tanto a degradação quanto as propriedades reológicas. A quantidade de líquido pode ser reduzida a um mínimo possível. Nesses casos, todas as formulações formadoras de apatita parecem pastas mais viscosas e facilmente moldáveis, porém, dificultam ou impedem a injetabilidade (DOROZHKIN, 2018).

Segundo Lanao (2011), incorporar macroporos (poros >100 μm) ao CPC, aumentando a área de superfície, é uma alternativa para fomentar a degradação. Vários métodos estão descritos na literatura para criação de redes interconectadas de macroporos incluindo a adição de partículas biodegradáveis, cristais solúveis em água como bicarbonato de sódio, manitol, sal ou glicose, técnicas rápidas de prototipagem e, adição de agentes espumantes (BIGI et al., 2004; HABRAKEN et al., 2008; LANAO et al., 2011; LODOSO-TORRECILLA et al., 2018).

1.5 ESPUMA COMO PRECURSORA DA MACROPOROSIDADE

Um dos métodos possíveis para introduzir a macroporosidade no CPC é através da adição de espuma ou pela geração de gás através de uma reação química. O principal benefício da introdução de macroporos por agentes espumantes

é a facilidade do método. A espuma, geralmente formada separadamente, é composta por soluções contendo agentes surfactantes que estabilizam a interface líquido-gás entre a suspensão e as bolhas de ar incoporadas por agitação, diminuindo a tensão superficial, tornando a solução mais estável.

Zhang et al. (2016) adicionaram espuma ao CPC e obtiveram tamanhos de poros interconectados entre 100 à 400μm e porosidade maior de 60%. Almirall et al. (2004) obtiveram alta porosidade (até 66%) controlando diferentes parâmetros de processamento, como a razão L/P e a concentração da solução de peróxido de hidrogênio. Real et al. (2002) usaram uma reação baseada em ácido entre NaH_2PO_4 e $NaHCO_3$ para formar bolhas de CO_2 em CPCs. Com esse método, foi alcançada uma porosidade de até 50%.

Estudo em tibiais de cabras mostrou significativa formação óssea para CPCs macroporosos em comparação com controles (CPCs sem macroprosidade). Com 10 semanas, enquanto os CPCs de controle ainda mantinham sua integridade, os CPCs macroporos degradaram quase por completo ao mesmo tempo houve neoformação óssea (REAL at al., 2003). Estudos adicionais demonstraram as capacidades de rege-neração óssea de CPCs com adição de espuma em modelos de animais, como ratos (HUSE, 2004) ou coelhos (JANSEN, et al. 2005; KROEZE-DEUTMAN et al., 2005). Além disso, vários estudos têm utilizado CPC com macroporosidade para carrear células endoteliais e osteoblastos (CHEN et al., 2014; THEIN-HAN., 2013).

1.6 POROSIDADE E TAMANHO DE POROS

A porosidade e o tamanho dos poros são pilares importantes nos CPC, uma vez que os macroporos (tamanho do poro 100-325μm) auxiliam no processo de degradação e neoformação óssea, e melhoram o intertravamento mecânico entre o tecido ósseo e o cimento. Os microporos (tamanho dos poros <10μm) auxiliam na absorção e liberação de substâncias, transporte de nutrientes e resíduos metabólicos pela circulação de fluidos biológicos quando a porosidade for interconectada (LODOSO-TORRECILLA et al., 2021).

Uma taxa de degradação mais rápida é atribuída a um tamanho maior dos poros devido à maior dispersão de produtos ácidos durante a degradação. Embora vários relatos tenham mostrado os efeitos do tamanho do poro, forma e porosidade na neoformação óssea, alguns relataram sobre a influência de porosidade

heterogênea na degradação, propriedades mecânicas e angiogênese (ABBASI et al., 2020).

Boccaccio et al. (2016) mostraram maior crescimento celular e transporte de nutrientes e resíduos na região altamente porosa. Sobral et al. (2011) avaliaram a eficiência do carreamento de células de uma célula de osteossarcoma humana em suporte ósseo tridimensional com dois tamanhos de poros: 100 e 700μm. Os suportes macroporosos (100 e 600μm) permitem uma melhor integração com o tecido ósseo hospedeiro, vascularização subsequente e distribuição óssea. O aumento do tamanho dos poros aumenta a permeabilidade, o que aumenta o crescimento ósseo (ABBASI et al., 2020).

1.7 INJETABILIDADE/COESÃO

Para serem injetáveis e aplicados em procedimentos minimamente invasivos, os CPCs devem ter duas propriedades: injetabilidade e coesão. A injetabilidade é a capacidade de um CPC passar por uma seringa de um determinado diâmetro e comprimento a uma determinada carga (por exemplo, 100N) de forma homogênea (KHAIROUN et al., 1998; BOHNER, 2005; ORÉFICE et al. 2012). A medição quantitativa pode estar relacionada à quantidade relativa de cimento extrudado da seringa.

A injetabilidade dos CPCs pode ser influenciada pelo tipo de seringa, tamanho da agulha, tamanho e forma das partículas (predominância para tamanhos diversos e esféricas), distribuição das partículas (desaglomeradas), razão L/P e viscosidade do líquido (LIVINGSTON et al. 2002; BOHNER, 2005, 2006; ZHANG et al., 2014). Dentre os fatores que afetam a injetabilidade, o uso de soluções viscosas como fase líquida é a melhor maneira de intensificar essa característica e evitar o fenômeno de filter-pressing, porém isso compromete o tempo de presa dos cimentos (BOHNER, 2005; O'NEILL et al., 2017).

O tempo de presa do CFC também pode afetar a injetabilidade: longos tempos podem causar separação da fase líquida da parte sólida da pasta cimentícia efeito (filter-pressing), provocada pela pressão exercida para injetar o material; entretanto, curtos tempos de presa podem provocar endurecimento do cimento dentro da seringa reduzindo sua injetabilidade (RAMALHO, 2010).

A coesão é a capacidade do cimento solidificar em um fluido sem se desintegrar. Foi descrito que os CPCs tem propriedades de coesão pobres, o que pode levar a desintegração de partículas no local ou na corrente sanguínea. Diferentes abordagens para melhorar a coesão do CPC incluem a redução do tamanho das partículas de CaP (BOHNER, 2006) ou o uso de CPC com alta viscosidade (BOHNER, 2000).

A incorporação de polímeros solúveis na matriz do CPC tem se mostrado uma alternativa para melhorar a injetabilidade, coesão e resistência mecânica. Biopolímeros naturais como quitosana, gelatina, colágeno, carboximetilcelulose (RAMIREZ et al., 2021) e alginato de sódio tem sido utilizados como aditivos (SHI et al., 2019; ZHONG et al., 2021).

O alginato de sódio é um sal monovalente do ácido algínico com propriedades como gelificante, espessante e estabilizante em meio aquoso (HAY et al., 2010). Além de biodegradável, estudos indicam que o alginato possui comportamento biocompatível e tem sido utilizado como material de partida para o desenvolvimento de tecidos sintéticos voltados à regeneração e substituição da cartilagem e de tecidos musculares, bem como em sistemas de encapsulação e liberação controlada de medicamentos (SANTOS, 2017). Sendo assim, o objetivo deste trabalho foi desenvolver e caracterizar um cimento com propriedades que favoreçam ao máximo a regeneração óssea.

2 OBJETIVO

O objetivo do presente trabalho foi desenvolver um cimento em forma de espuma constituido pela fase alfa do fosfato tricálcico com diferentes proporções de sulfato de cálcio e caracterizar sua porosidade e tamanho de poros, estrutura, morfologia e bioatividade em fluido corporal simulado (SBF).

3. ARTIGO

Material Science and Engineering C

Development and characterization of a foamed cement based on α-tricalcium phosphate and calcium sulfate for bone regeneration

ABSTRACT

Calcium phosphate cement (CPC) has been widely studied as a synthetic biomaterial alternative for bone regeneration. Injectability allows repairing small and irregular bone defects with minimally invasive acess and reducing surgical time. CPC should degrade at an appropriate rate to allow bone neoformation simultaneously. The degradation rate depends on the properties of CPC such as molar ratio calcium/phosphate (Ca/P), crystalline structure, surface area, porosity, and pore size. A sufficiently porous pathway, with interconnected pores, is necessary to allow the formation of blood vessels and osteoprogenitor cells proliferation. The aim of this study was to prepare and characterize a foamed cement based on the alpha phase of tricalcium phosphate (α-TCP) and calcium sulfate hemihydrate (CSH). The proportions between α-TCP/CSH wt% were: 90/10wt.% (G90), 80/20wt.% (G80), 70/30wt.% (G70) respectively. One group remained without CSH to be used as control. The liquid phase was composed of sodium hydrogen phosphate, a surfactant, sodium alginate and distilled water. The foam was obtained using syringes joined by a PVC connector, so that the liquid phase and air were quickly mixed by pushing the two plungers of the syringes alternately in opposite directions. Subsequently, the foam volume was pumped into another syringe containing α-TCP and CSH powder until a homogeneously foamed cement was formed. The characteristics evaluated were pore size, porosity, crystallographic and morphological structure, bioactivity, and pH. X-ray computed microtomography (micro-CT) images of all samples revealed a random distribution and wide size variation of pores ranging from 10μm to 1mm. X-ray diffraction (XRD) analysis showed calcium deficient hydroxyapatite (CDHA) peaks increased in all groups with completed hydrolysis reaction of CSH after immersion in a solution that simulates body fluid (SBF). Observations by Scanning Electron Microscopy (SEM) confirmed the XRD and Fourier- transformed infrared (FTIR) results and showed a superficial variation between the groups at different immersion times. G90 and G80 exhibited more defined petaloid forms of CDHA after immersion in SBF. Biphasic cements (α-TCP/CSH) showed a higher percentage of pore ($p<0.05$) than the α-TCP group without CSH. The cements groups consisting of α-TCP and CSH showed desirable and promising characteristics for bone regeneration. Biocompatibility and *in vivo* studies are necessary to confirm these findings.

Keywords : Injectable cement; foamed cement, calcium phosphate; calcium sulfate; porosity; bioactivity, SBF.

3.1 Introduction

Many researchers have sought a new synthetic product based on biomaterials developed for bone repair and regeneration. These biomaterials include metals, polymers, ceramics, bioactive glasses, calcium sulfates, calcium carbonates, and calcium phosphates (CaPs). The current challenge is to find an injectable material that can be molded into the desired shape and size of the bone defect, with cohesive stability and excellent contact between bone and graft, hardening at body temperature. Calcium phosphate cement (CPCs) are promising for these clinical applications due to their properties such as the ability to form an injectable paste that can self-set and harden *in situ* to form a scaffold through a dissolution-precipitation reaction [1] in minimally invasive procedures [2,3,4].

CPC was introduced by LeGeros in 1982 [5] and the first patent for self-setting was obtained by Brow and Chow in 1983 [6]. Nowadays, CPCs represent one of the most widely studied synthetic biomaterials due to their crystalline structure and chemical composition similar to the inorganic phase of bone tissue, biological hydroxyapatite [7]. In addition to benefits such as biocompatibility, bioactivity, biodegradability [2, 8,], osteoconductivity, some may even have osteoinductive potential [9, 10].

A series of CaPs are available in different phase compositions such as hydroxyapatite (HA), β-tricalcium phosphate (β-TCP), and α-tricalcium phosphate (α-TCP). CPC based on α-TCP is of special interest due to their self-setting behaviour when mixed with an aqueous liquid phase. The reaction occurs through the dissolution of Ca^{2+} and PO_4^{3-} ions into the liquid phase: $3Ca_3(PO_4)_2 + H_2O \rightarrow 9Ca^{2+} + 6PO_4^{3-} + H_2O$. Subsequently, the solution becomes supersaturated with apatite, leading to the formation of an entangled network of precipitated calcium deficient hydroxyapatite (CDHA) crystals: $9Ca^{2+} + 6PO_4^{3-} + H_2O \rightarrow Ca_9HPO_4(PO_4)_5(OH)$ [11].

These setting reactions are known as dissolution-precipitation reactions [12, 13] CDHA is similar to the mineral phase of bone and teeth. The apatitic phase will ensure bone conductivity in the defect. Among other properties, this cement does not retract or expand, and does not release heat during the setting reaction [14,15].

It is accepted that pure α-TCP cement needs further improvements to broaden their potential clinical applications. Despite the similarity to bone tissue, the end setting product, CDHA, has a drawback it is so stable in vivo that bone cement resorption takes a long time, 1-2 years [16]. To accelerate cement absorption, several authors have found various ways of improving macroporosity with a greater number of larger pores in apatitic cements [17,18,19].

Calcium Sulfate (CS) has, over 100 years of clinical history as a bone substitute, being one of the most successful bone cements because it can harden *in situ* without causing inflammation [20]. It can promote bone healing due to the level of calcium ion concentration and can be used like as a source of rapid-release calcium [21]. CS has good biocompatibility, degradability and injectability [22, 23, 24]. However, CS cannot meet the requirement of clinical injectable operating time (about 5-15 min) in a single phase and Its degradation rate is faster than bone regeneration [25]. Modifying the L/P ratio, chemical and phase composition, degree of crystallization and/or porosity, can be alternatives to adjust its degradation rate. In addition, foaming agents can be introduced into the liquid phase to modify porosity and injectability [26].

Adding Calcium Sulfate Hemihydrate (CSH) is an absorption phase alternative to improve hardenig and biodegradation rate. Is supposed to produce macropores to favors bone tissue ingrowth into CPC after dissolution by body fluids [27] and further osteoconduction [28]. The addition of CSH in the composition of α-TCP forms a biphasic cement that sets due to the hydration reactions of both main reactants, i.e., α-TCP into CDHA and CSH into CSD (calcium sulfate dihydrate): $CaSO_4 \cdot ½H_2O$ + 3/2 $H_2O \rightarrow CaSO_4 \cdot 2H_2O$.

Thus, in view of the previous arguments regarding the desirable characteristics of a material for bone regeneration, the objective of this study was to prepare a foamed injectable cement of α-tricalcium phosphate and calcium sulfate. The porosity and pore size, structure, morphology and bioactivity in simulated body fluid were further investigated.

3.2 Materials and Methods

3.2.1 Materials

All purchased compounds applied in this study were analytically pure. The α-TCP powder synthesis and the liquid phase used in this study was performed by Biomaterials Laboratory Labiomat, Materials Department, Engineering School of Federal University of Rio Grande do Sul (UFRGS). The synthesis was performed by wet precipitation using precursors with [Ca^{2+}] and [PO_4^{3-}], maintaining the Ca/P ratio at 1.5. The procedure consisted in an acid-base reaction, where 0,5M of dibasic ammonium phosphate [$(NH_4)_2(HPO)_4$] (Dinâmica Ltda) solution was added to 0,5M of calcium nitrate tetrahydrate [$Ca(NO_3)_2{\cdot}4H_2O$] (Sigma Aldrich, ACS) solution, previously heated to a temperature of 60°C in a round bottom distillation flask with constant stirring of 170 rpm. The flow rate of the phosphate solution was fixed at 14mL/min. The precipitate was filtered and dried in an oven at 100°C for 24 hours. After drying, the material was manually crushed in a porcelain mortar. The powder was then thermally treated in an alumina crucible at 1400°C for an hour. The heating rate was 5℃/min until the plateau was reached. The powder remained in the oven until it reached room temperature. Finally, the material was ground again in the mortar and sieved through a #325 mesh. To compose the solid phase, CSD was heated for 24 h at 110°C for the formation of CSH [29].

The liquid phase was constituted by a setting accelerant disodium hydrogen phosphate dodecahydrate (Na_2HPO_4 •12 H_2O-Synth), a surfactant Lutensol ON110, and sodium alginate hydrogel ($C_6H_7NaO_6$ - Sigma-Aldrich) as a rheological promoting agent.

3.2.2 Methods

3.2.2.1 Cement Preparation

The foamed injectable cements were prepared mixing α-TCP (90, 80 or 70%) and CSH (10, 20, or 30wt.%), respectively. A group with 100 wt.% α-TCP was used as control, totaling four groups (Table1).

Table1 The prescription of injectable α-TCP/CSH composite cement

Symbol	Power phase (P)	Liquid phase (L)	L/P (mL/g)
G70	70 wt.% α-TCP 30 wt.% CSD	6.25 wt.% Na_2HPO_4 4.3 wt.% Lutensol 2wt.% Alginate	0.6
G80	80 wt.% α-TCP 20wt.% CSD	6.25 wt.% Na_2HPO_4 4.3 wt.% Lutensol 2 wt.% Alginate	0.6
G90	90 wt.% α-TCP 10 wt. % CSD	6.25 wt.% Na_2HPO_4 4.3 wt.% Lutensol 2 wt.% Alginate	0.6
G100 (CONTROL)	100 wt.% α-TCP powder	6.25 wt.% Na_2HPO_4 4.3 wt.% Lutensol 2 wt.% Alginate	0.6

An aqueous solution containing distilled water, 6.25wt.% Na_2HPO_4, 2% sodium alginate and 4.3wt% surfactant Lutensol ON 110 was mixed uniformly to obtain a foam [29]. The solution was transferred with a micropipette in a commercial syringe (volume: 3ml, inner diameter: 8mm, and nozzle diameter: 2mm). Subsequently, the volume of air (3ml) was pumped into another syringe containing the Na_2HPO_4 solution. Both syringes were joined by a PVC connector, and the solution and air were rapidly mixed by pushing the two plungers of the syringes alternately in opposite directions for thirty seconds until a homogeneous foam was formed (Fig. 1, step 1). The Liquid/Powder (L/P) ratio was 0.60 mL/g, kept the same for all cements. Subsequently, the volume of foam was pumped into another syringe containing α-TCP and CSH powder. Both syringes were joined by a PVC connector, and the foam and powder were rapidly mixed by pushing the two plungers of the syringes alternately in opposite directions for fithteen seconds until a homogeneous foam cement was formed (Fig. 1, Step 2). The resultant paste was placed into a polivinilsiloxano mold with a diameter of 6.0 ± 0.1mm and a height of 2.0 ± 0.1mm for microCT analysis, and into a mold with a diameter of 10.0 ± 0.1mm and a thickness of 3.0 ± 0.1mm for bioactivity measurement *in vitro*. The samples were kept in 100% relative humidity at 37°C for 24h.

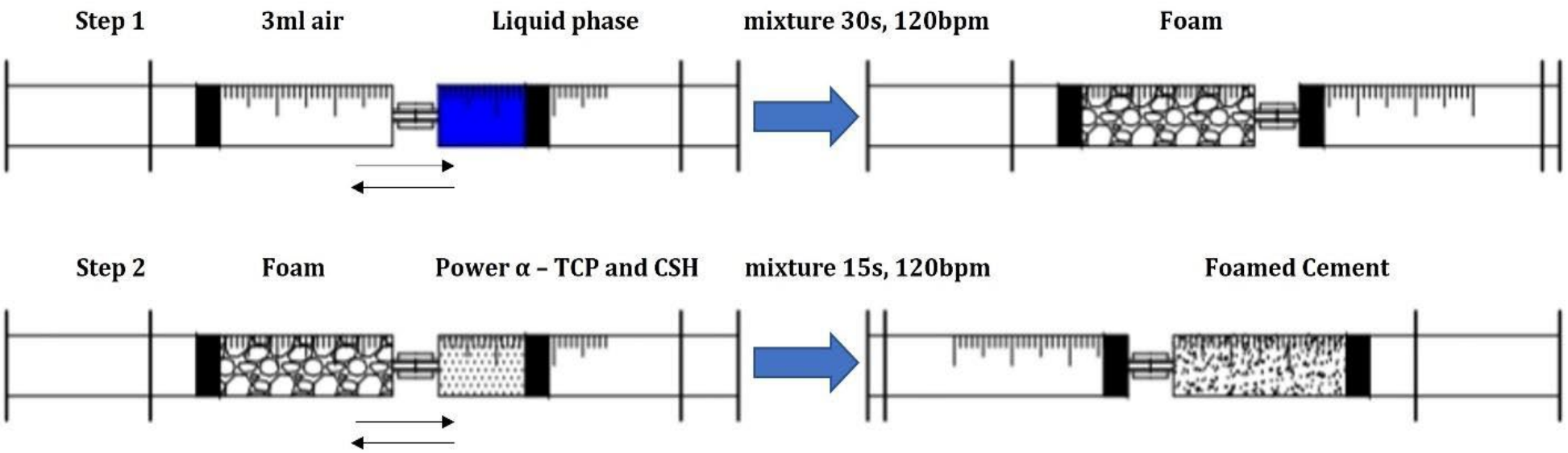

Fig. 1. Schema showing the prepariation process of the foam liquid phase and foamed cement phase.

3.2.2.2 X-ray diffraction (XRD)

The crystal structure phase compositions were examined by quantitative X-ray diffraction. α-TCP and CSH powders were individually analyzed. The cement samples were prepared and injected into the sample port to be analyzed immediately (0h), after 1, 6, and 24h and after being 7 and 21 days in SBF. All results were compared with the crystallographic sheet of ICSD Database. A Rigaku, ULTIMA IV X-ray diffractometer (Tokyo, Japan) based on monochrome RS CuKα radiation (λ = 1.5405 Å, 20 mA, 45 kV) in a continuous scan mode, was used. The 2θ range was from 10° to 70° at a scanning speed of 2°/min.

3.2.2.3 Fourier- Transform Infrared (FTIR)

α-TCP and CSH powders were analyzed by FTIR-ATR (Vetrex 70, Bruker Alpha, Ettingen, Germany). The powder was dispensed on the ATR crystal in a polyvinylsiloxane matrix with a 4mm diameter and 1mm thickness. Subsequently, each experimental cement was prepared, positioned on ATR in the polyvinylsiloxane matrix, and the setting kinetics was analyzed for 24 hours in a humid environment surrounded by wet gases. Identifications of functional groups and characteristics of chemical bonds were informed. Data were evaluated with Pos 6.5 software (Bruker Optics, Ettlingen, Germany) with Blackman Haris 3-Term apodization, in the spectrum from 4000-400 cm^{-1} range with 64 scans at 4 cm^{-1} resolution. Spectra were obtained at different time points (0, 20, 40, 50min; 1, 6 and 24h).

3.2.2.4 Bioactivity in SBF / Degradation

SBF was prepared according to the method proposed by Kokubo et al [30], dissolving sodium chloride (NaCl – 2.008g), sodium hydrogen carbonate ($NaHCO_3$ – 0.087g), potassium chloride (KCl – 0.056g), di-potassium hydrogen phosphate trihydrate (K_2HPO_4 $3H_2O$ – 0.057g), magnesium chloride hexahydrate ($MgCl_2$ $6H_2O$ – 0.077g), Hydrochloric Acid (HCl 1M – 9.75ml), calcium chloride ($CaCl_2$ – 0.075g) and sodium sulfate (Na_2SO_4 – 0.018g) into 175ml of deionized water and buffering the

solution to a pH of 7.4 by tris (hydroxymethyl) aminomethane $(CH_2OH)_3CNH_2$ – 1.529g) and HCl at 36,5℃.

After setting, samples (10.0 ± 0.1mm diameter and 3.0 ± 0.1mm thickness) were weighed (W_0) before being immersed in 3ml of SBF solution and kept incubated at 36.5ºC ±0.5ºC for 7 and 21 days. SBF was replaced every week. All samples were gently rinsed with deionized water, dried in a desiccator without heating for 24 h, and then weighed (Wi) by electronic analytical balance with an accuracy of 0.0001g (AUW220D, Shimadzu, Kyoto, Kyoto, Japan).

The degradation or the weight loss percentage $Wl(\%)$ of the samples was calculated using the following equation:

$$Wl(\%) = (W_0 - Wi)/W_0 * 100,$$

where W_0 was the initial weight, and Wi is the weight after immersion in SBF.

3.2.2.5 pH measurement

The pH values of the SBF solution were measured at 0, 0.5, 60, 360min and 1, 7, 14, and 21 days with an electrolyte type pHmeter (DIGIMED – DM23- São Paulo, SP Brazil). Each average pH value was obtained from 4 measurements taken under the same testing conditions.

3.2.2.6 X-ray computed microtomography (micro-CT)

Three samples per group were scanned before being immersed in SBF using a micro-CT machine (SHIMADZU - inspeXio SMX-90CT Plus Micro Focus X-Ray CT System3D, Tokyo, Japan). The microfocus X-ray operated at 80 kV and 100μA with a Voxel Size 0,018 mm/pix). About 540 cuts per sample were generated. The reconstructed 2D images, which were compiled and analyzed to generate 3D images, were processed with CTAn® software (Bruker-Massachussets, USA). A customized processing was applied to the regions of interest (ROI) in the samples to measure pore sizes using the RadiAnt DICOM Viewer 2021.2 software.

3.2.2.7 Pore size distribution

The pore size distribution was measured randomly, n=100, in three samples from each group, based on the images obtained by *micro-CT* using RadiAnt DICOM VIEWER software. The image was divided into 4 quadrants, where in each, 25 pores were measured, totaling 100 measurements. All analyzed ROI were in the central cross section of the microtomography to ensure that the analyzed area was always the same or relatively close. In some samples, half a pore appeared at the edge, and this was not accounted for.

3.2.2.8 Porosity

Three samples per group were dried after immersion in SBF for 21 days, to determine their porosity. The porosity of each group (G70, G80, G90 and G100) was calculated as percentual ($P_{\%}$). It was calculated by a geometric method using the following equation:

$$\mathbf{P_{\%} = 1 - (\rho_f / \rho_{theoretical}) \times 100}$$

Where: $\boldsymbol{\rho_{theoretical}}$ is the density calculated using the following equation:

$\%V_{CDHA} = V_{CDHA} / (V_{CDHA} + V_{CSD})$

$\%V_{CSD} = V_{CSD} / (V_{CDHA} + V_{CSD})$

$\boldsymbol{\rho_{theoretical}} = (\%V_{CDHA} \times \rho_{CDHA}) + (\%V_{CSD} \times \rho_{CSD})$

and

$\boldsymbol{\rho_{CDHA}}$ = 3,15 g/cm^3 (calcium deficient hydroxiapatite density)*

$\boldsymbol{\rho_{CSD}}$ = 2,32 g/cm^3 (calcium sulfate dehydrated density)**

$\boldsymbol{\rho_f}$ = apparent density of foamed CPC samples determined by dividing their weight by their volume.

*The density of calcium deficient hydroxiapatite after the setting reaction was determined by pycnometrics according to ASTM D854-14 Specific Gravity of Soil Solids by water Pycnometer, using 99,9% ethyl alcohol as the liquid medium [31].

**The density of calcium sulfate dehydrated was provided by the International Center for Diffraction Data (ICDD) plug 46-0905.

3.2.2.9 Scanning Electron Microscopy (SEM)

The surface morphology of one sample for each group was collected for microscopic observations before and after immersion, for 7 and 21 days in SBF. The samples were placed on metallic stubs and gold-sputter coated. SEM analysis (JEOL/EO JSM-6610 Germany) was performed under 10kV, at 50, 100, 300, 1000, 5000, 10000 magnification.

3.2.2.10 Statistical analysis

Statistical differences were evaluated by one-way Analysis of Variance (ANOVA), complemented by the multiple comparison Tukey test, where applicable. All analyses were performed considering a significance level of 5% or $p<0,05$.

3.3. Results and Discussion

3.3.1 X-ray diffraction

XRD diffractographs of α-TCP and CSH powders are shown in Fig. 2. A and B, respectively. Standard diffraction peaks of crystalline α-TCP and CSH were identified according to ICSD crystallographic sheet 000923 and 079528 respectively.

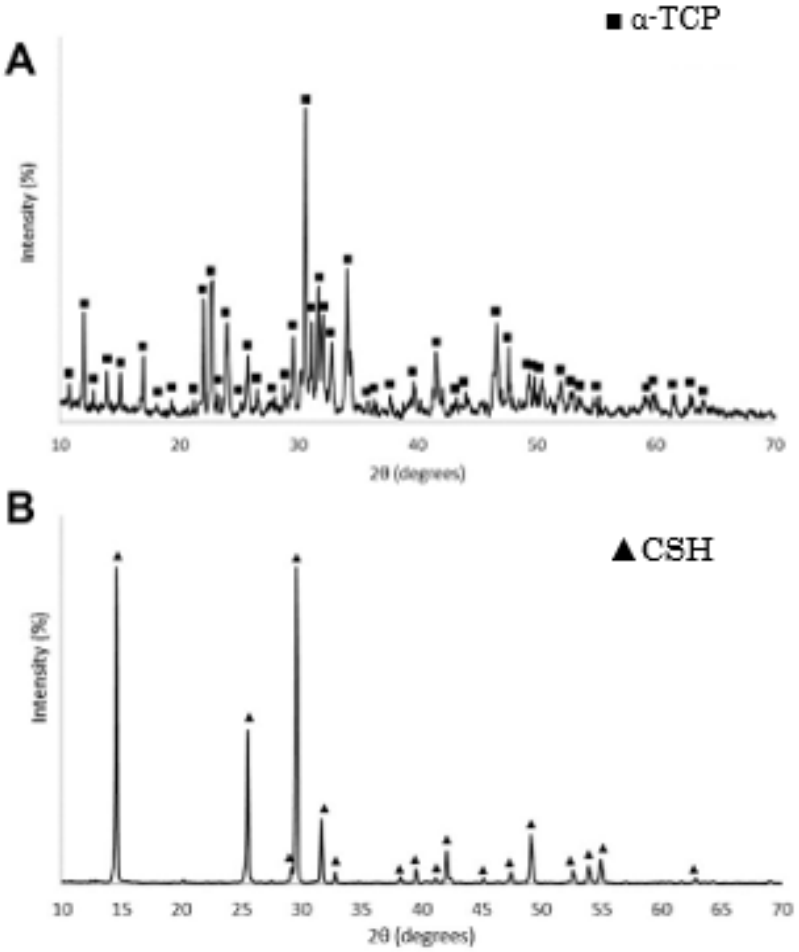

Fig. 2. XRD analysis of α-TCP and CSH powders. (A) XRD diffractogram of α-TCP powder showing the absence of peaks related to β-TCP and HA, common contaminations in the synthesis of α-TCP. (B) The XRD patterns of pure CSH.

The dissolution of crystalline α-TCP began immediately after the mixture in all groups (Fig.3a/3b). The same occurred with CSH in G70, G80 and G90. The cements were prepared before the first reading in the XRD and analyzed at 0, 1, 6, and 24h. During the setting time, α-TCP and CSH were not disappear. After setting for 24h, XDR showed that all samples investigated contained diffraction peaks of CDHA and CSD (except G100).

HARDENED SAMPLES (NON-IMMERSED in SBF)

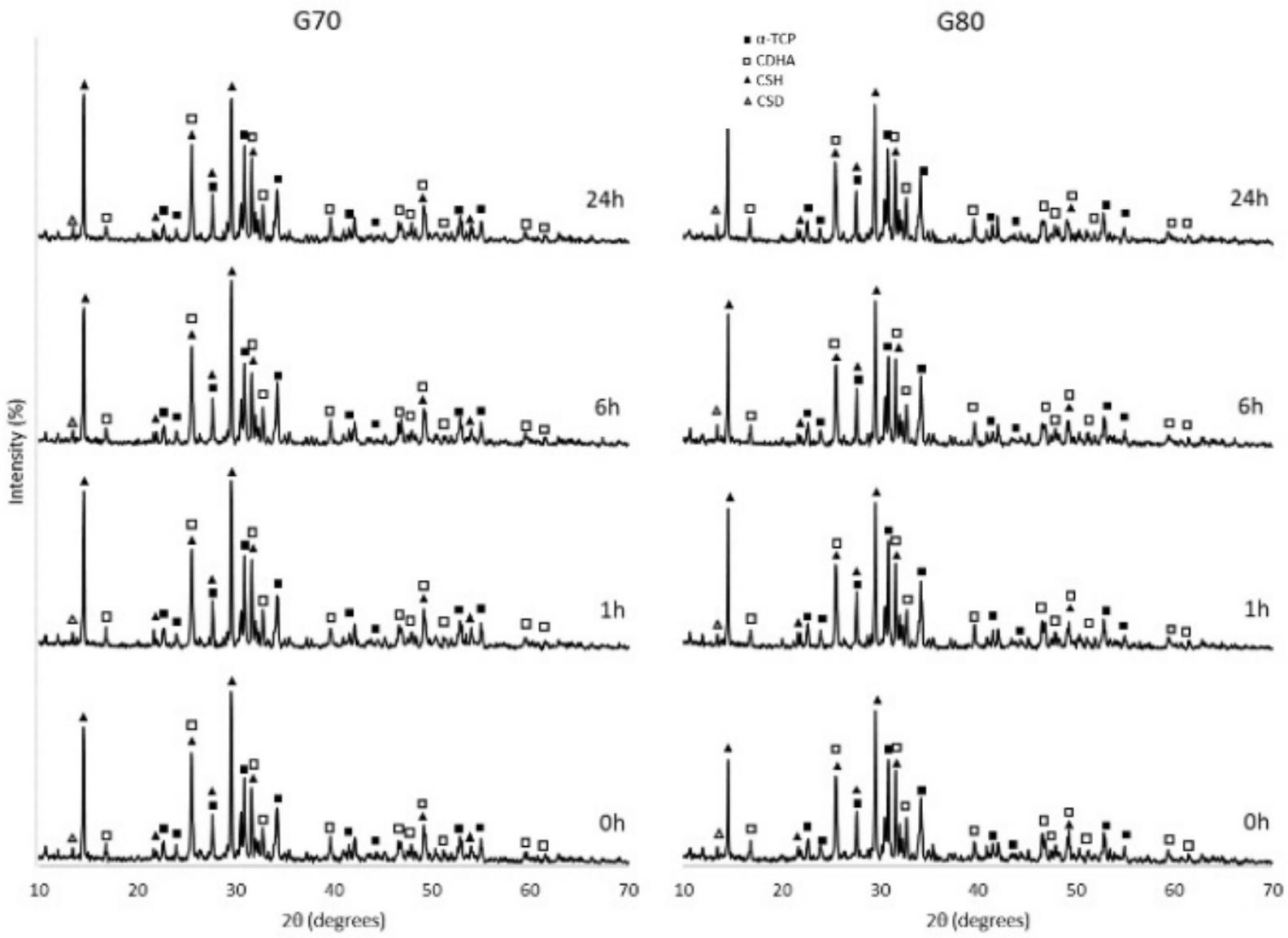

Fig. 3a - XRD diffratogram of setting reaction of all cement groups.

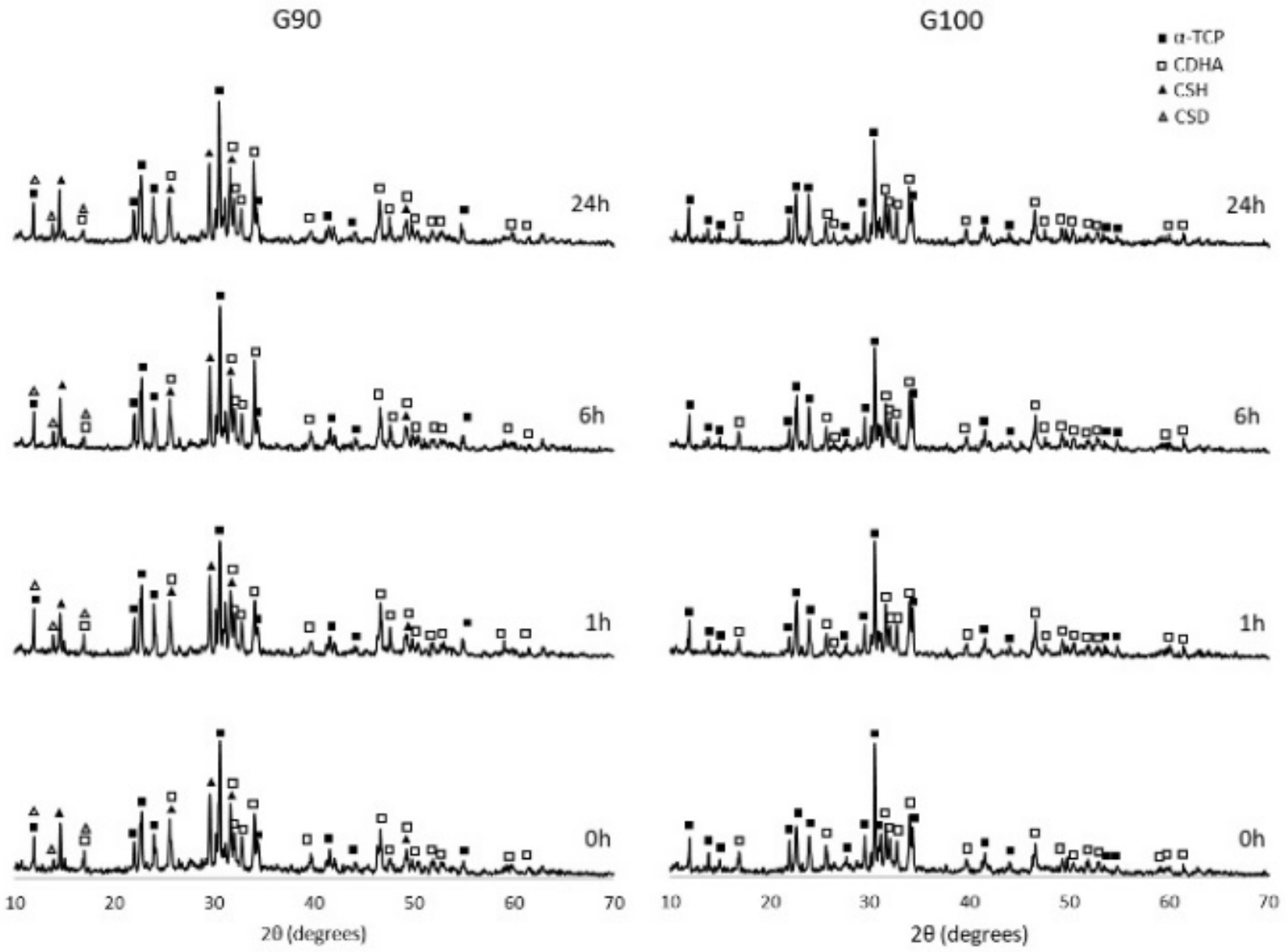

Fig. 3b - XRD diffratogram of setting reaction of all cement groups.

The results in Fig. 4a and 4b indicate that all cement samples showed CDHA formation in 7 days after SBF immersion. Only a very small amount of α-TCP was detected in all groups after 21 days. The intensity of this peak was very small in all samples, and did not depend on the presence of CSH or CSD. This demonstrated that the CSH addition did not affect the hydrolysis of the α-TCP. After 7 days, G70, G80, and G90 had completed the hydration reaction and formed CSD and after 21 days all CSD was degraded. The intensity of these characteristic peaks increased with increasing reaction time. These results suggest that the addition of CSH increased the saturation of phosphate ions in the cement paste, hence provoking a decrease of the dissolution rate of α-TCP and probable decrease of the transformation rate of α-TCP into CDHA. This was probably due to Hadley´s grain formation where the nucleus of α-TCP is surrounded by a CDHA layer, preventing the reaction of this material with the liquid (SBF). Another hypothesis is the increase in PO_4 saturation in the SBF, which would also decrease the dissolution of α-TCP. And the last hypothesis is that the setting reaction might require a long time to reach 100% conversion of α-TCP into CDHA even if the cement has a short setting time because the setting rate of the cement is not a constant value [32].

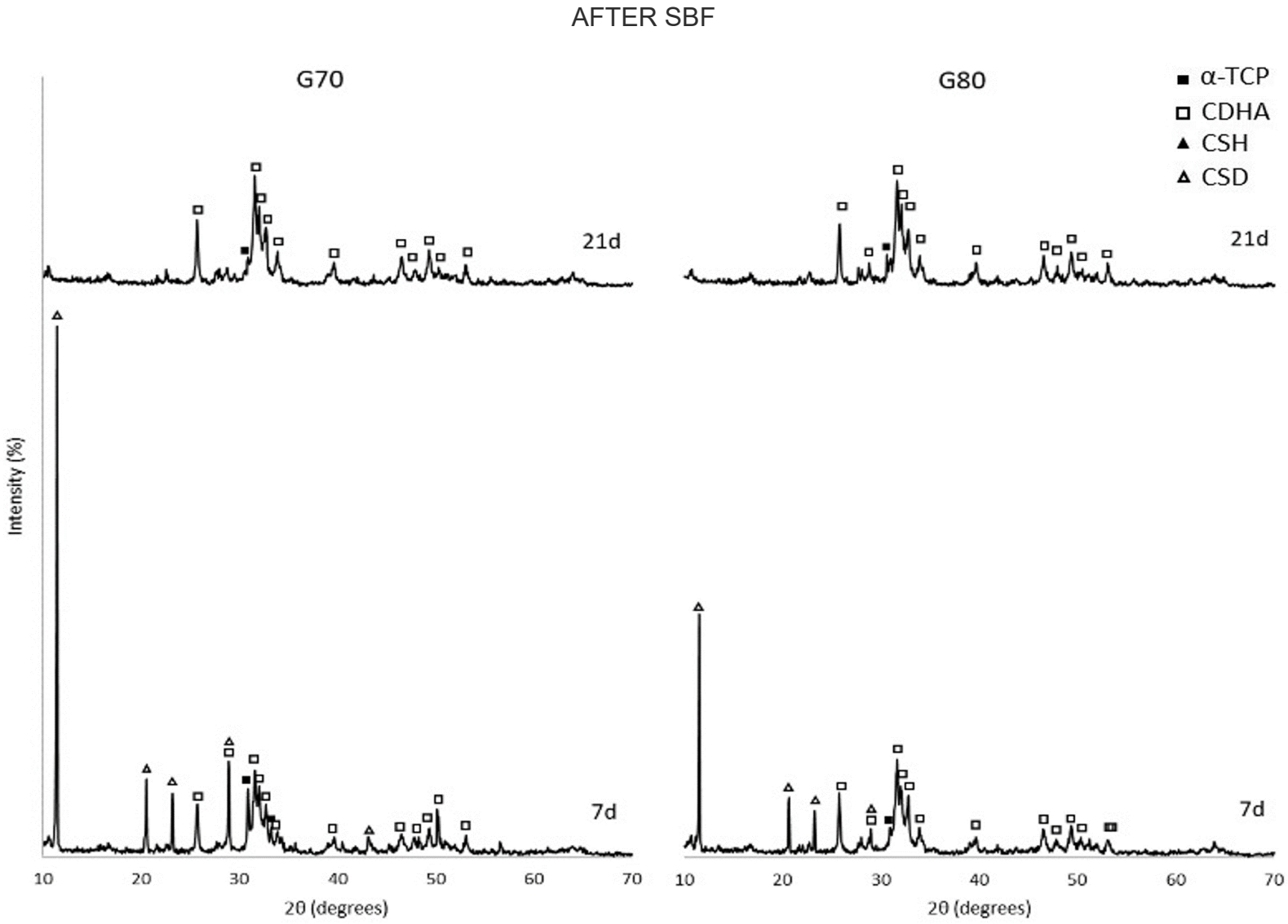

Fig. 4a – XRD diffratogram of all groups after 7 and 21 days in SBF solution

AFTER SBF

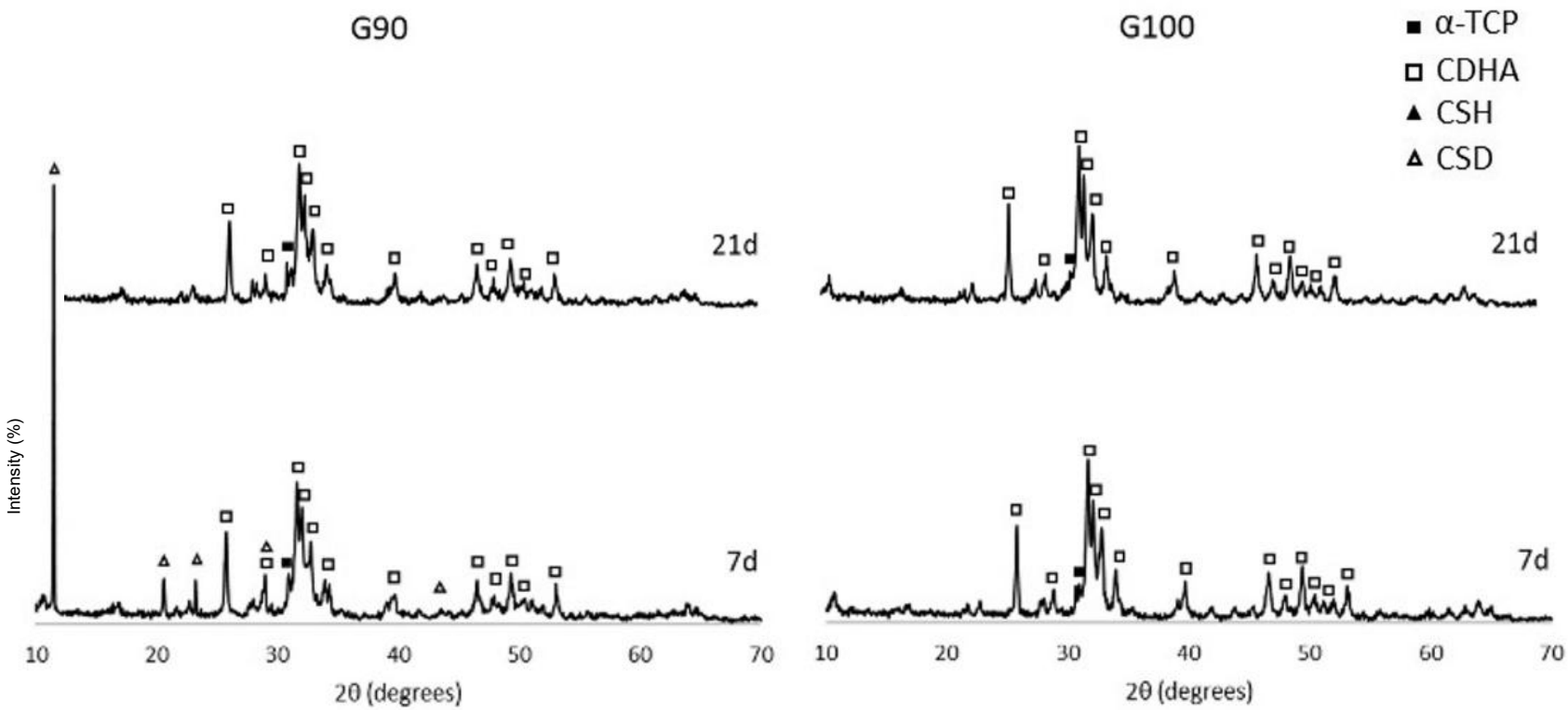

Fig. 4b – XRD diffratogram of all groups after 7 and 21 days in SBF solution.

3.3.2 Fourier- Transform Infrared (FTIR)

The FTIR spectrum of α-TCP and CSH powders is shown in Fig. 5. (A) FTIR spectra showed characteristic vibrations of phosphate groups at 454 cm-1 (symmetric P-O bending, v2), 563 cm-1 (anti-symmetric P-O bending vibration mode, v4), 597 cm-1 (Symmetric P-O stretching, v1) and 1025 cm-1 (anti-symmetric P-O stretching, v3) [33]. (B) FTIR spectrum in the wavenumber range 4000-400 cm-1 is in good agreement with those reported in the literature [34, 35, 36] S-O v4 is shown at 600 and 659cm-1. This behavior is very similar to that reported by Prasad [34] and Putnis [36].The peak around 1008 and 2326 cm-1 is related to S-O (v1), 1098, 1115, 1152 and 2338 cm-1 to S-O (v3) comparable with those of Prasad [34] CSH has IR-active mode in the bending mode of water O-H (v2) observed at 1622 cm–1. The other two stretching modes (v3 and v1) of water groups are found at 3610 and 3552 cm–1 [34].

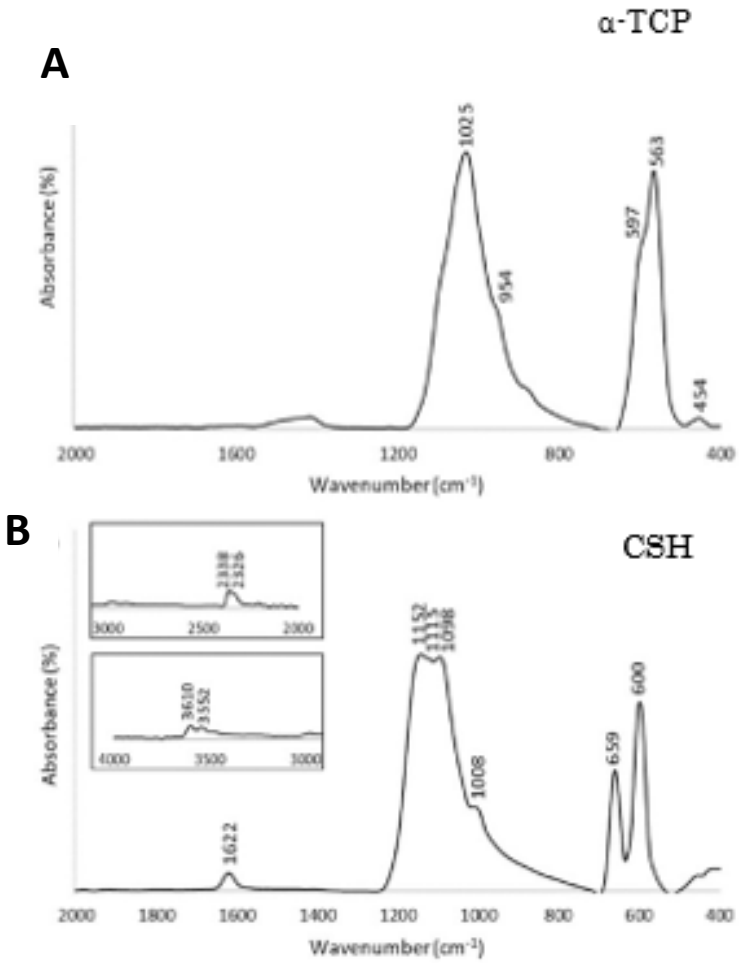

Fig. 5. FTIR analysis of α-TCP and CSH powders.

Fig. 6 shows the FTIR spectra of the setting reaction at 0, 20, 40min and 1, 6, and 24h. From the position and assignment of the peaks the following features can be pointed out: G70 shows the P-O (v_4) connection or PO_4^{3-} at 551 and 597 cm^{-1} typical of the FTIR of apatite. The peak at 1015 cm^{-1} should be attributed to u_3 phosphate modes, and the peak at 1055 cm^{-1} is attributed to P-O (u_4) and S-O (v_3) of the CSH. The peaks contained in the wavenumber 640 (v_1), 1627 (v_2), and 1622 cm^{-1} (v_2) are the vibration peak of the hydroxyl group [38]. The band in 3220-3378 cm^{-1} (v_3) is due to the H_2O adsorbtion. After 6h, G70, G80, and G90 showed peaks at 595(v_4), 1014(v_3), and 1086cm^{-1} (v_3) attributed to P-O [37], corresponding to CDHA. The band at 633(v_1), 1633(v_2), and 3291cm^{-1} [37] is due to the O-H and probably low CDHA precipitation. As the time increases, this band became less intense due to the water adsorption, the same occurred in G90 at 3296 cm^{-1} . The peak at 2338 (v_1+v_3) refers to S-O. After 24h, all groups presented peaks 450-600cm^{-1} and 900-1015cm^{-1} region indicating the completed setting reaction [37].

Calcium sulfate and α-TCP react with each other to create CDHA. Dissolution of $CaSO_4 \cdot ½H_2O$ on the α-TCP interface can lead to a partial substitution of phosphate groups (HPO_4^{2-}) in the CDHA structure ($Ca_9(HPO_4)_2(PO_4)_4(OH)_2$) via SO_4^{2-} [38]. The ionic radius of PO_4^{3-} ions varies from those of SO_4^{2-}, whereas the ionic radius of HPO_4^{2-} closely matches it (HPO_4^{2-}, 0.236 nm; SO_4^{2-}, 0.230 nm) [39]. Therefore, it may be assumed that CDHA was formed by the substitution of SO_4^{2-} by HPO_4^{2-} ions in the hydroxyapatite structure. The reaction can be as follows:

$$9CaSO_4 \cdot ½H_2O + 6HPO_4^{2-} + 3/2\ H_2O =$$

$$Ca_9(SO_4)_2(PO_4)_4(OH)_2 + 6H^+ + 7SO_4^{2-} + 2HPO_4^{2-} + 16H_2O$$

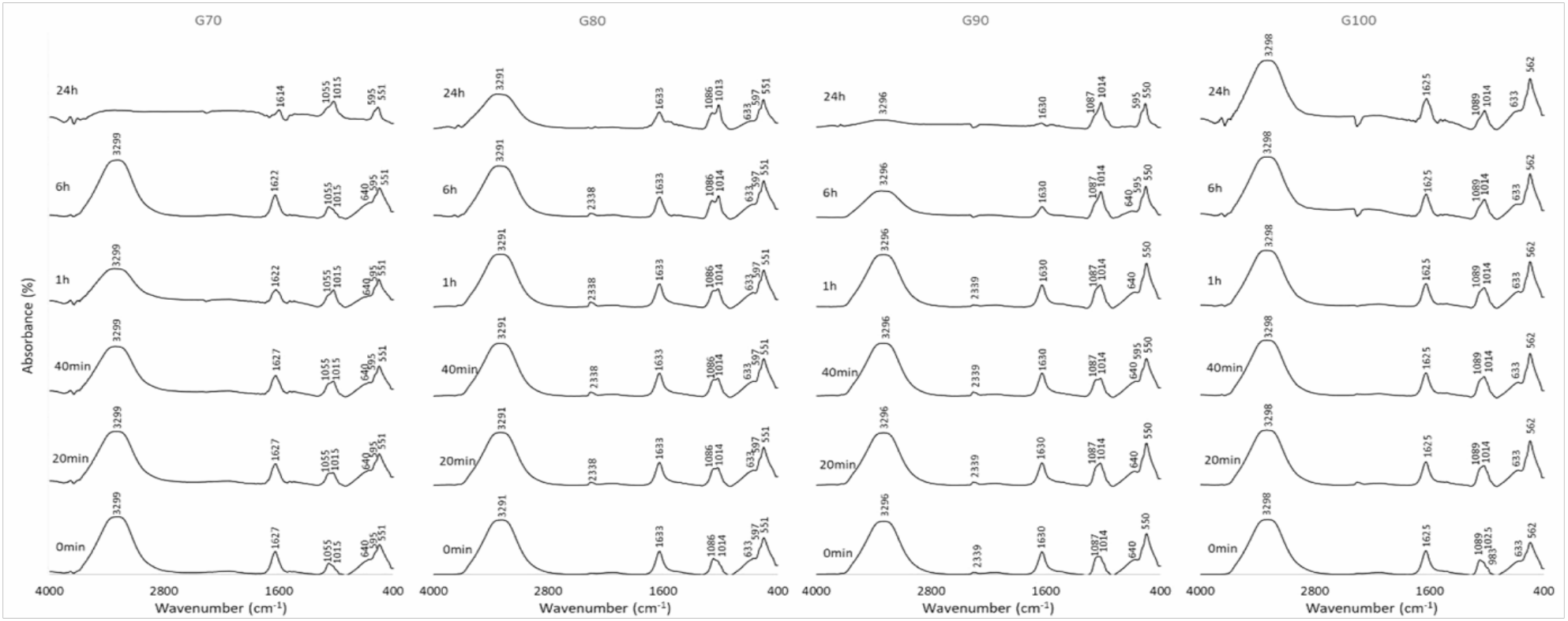

Fig. 6. FTIR spectra of setting reaction at 0, 20, 40 min and 1, 6, and 24h of CPC groups.

3.3.3 Pore Size Distribution

In all groups, micro-CT confirmed the random pore distribution throughout the sample (Fig.7). The pore size showed a heterogeneous range from 10 µm to 1 mm, (Fig. 7)

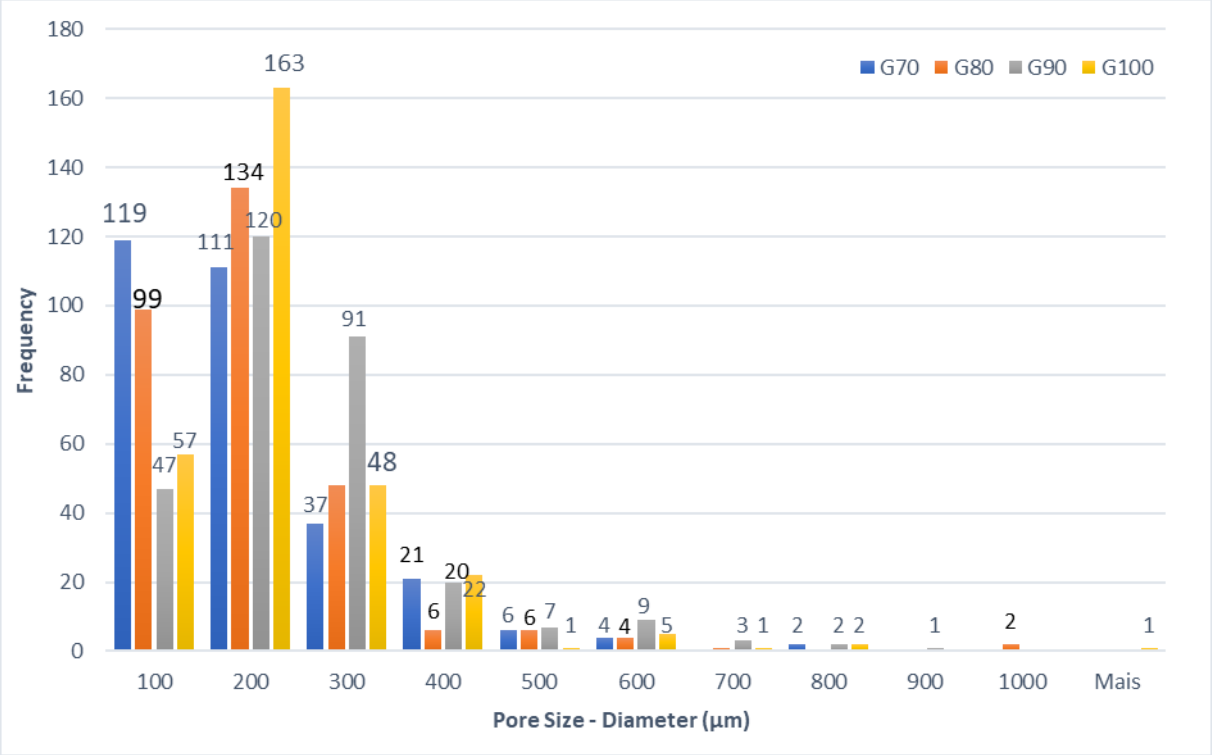

Fig. 7 – Histogram of the frequency of pore diameter distribution. (hardened and non-immersed samples)

3.3.4 *Porosity*

The porosity of the foamed cements manufactured in this study ranged from 33 (±1)% to 52 (±1)%. These values are below the values reported by Montufar et al [40] and Zhang [41]. Montufar et al [40], used a domestic food mixer to obtain the foam with an L/P ratio of 0.50 and 0.65 mL/g. They found 61.9% and 75.8% of total porosity, respectively [40]. Although the L/P ratio used in this study (L/P = 0.60mL/g) is higher than that reported in the literature for medical applications (L/P = 0.32mL/g),

it should favor the increase in cement porosity [8]. Almirall [42] foamed an α-TCP cement with a H_2O_2 solution and obtained the total porosity ranging between 45% and 48%, and the differences observed could be attributed to the different processing parameters.

The foamed process used in the present study was shown in a previus research study [41]. They used the foamed method by seringes and showed 75 and 80% of total porosity with 0,60 and 0,80mL/g, respectively. However, the authors find macropores with sizes over 300μm only in the foamed CPC with a total L/P ratio of 0,8. Compared to the same L/P ratio (0.60 mL/g), our study obtained pores with sizes greater than 300 μm.

Tab. 2. shows the porosity percentage of the groups after 21 days immersion in SBF. The analysis of these results showed that, 10, 20 or 30% of calcium sulfate hemihydrate added to CPC, significantly increases the percentage of porosity when compared to the G100 (pure α-TCP). Thus, the increase in porosity can be attributed to the presence of CSH.

Table 2 Porosity percentage (P%) of groups after 21 days immersion in SBF. (Tukey Pairwise Comparisons - 95% Confidence.)

Groups	n	P (%)	Factor
G70	3	50 ±3,6	A
G80	3	51,67 ± 0,5	A
G90	3	52 ± 1	A
G100	3	33 ± 1	B

Means that do not share a letter are significantly different (p<0,05).

The experimental foamed cement maintained the macropores after injection and after hardening (Fig.8) proving the effectiveness of the foaming strategy. The presence of pores in CPC is beneficial for its degradation. Macropores on the order of 100 - 600 μm are present in all cement group. These diameters corroborate Abbasi et al [45]. Osteoblasts prefer larger pores for regenerating mineralized bone. This allows macrophages to infiltrate, eliminate bacteria, and induce the infiltration of other cells involved in colonization, migration, and vascularization *in vivo* [45]. A

faster degradation rate is attributed to a larger pore size because of the greater dispersal of acidic products during degradation. Considering [46] results a pore size of 100 to 325μm was optimal for bone engineering scaffolds *in vitro*, G90 and G100 presented the highest percentage of pores between these measurements, 77 and 77.66% respectively.

The least pore size found was 11,60 μm in G80, but G70 was the group with more micropores. Pore size < 10μm creates a larger surface area that stimulates greater ion exchange and bone protein adsorption [47]. Murphy et al [48] suggest that the best pore size for initial cell adhesion was 95 μm *in vitro.* According to Rustom et al [49], biphasic calcium phosphate with a micropore (<20μm) size of 2.2 μm and macropores (>300 μm) with a size range of 650–750 μm ensures a homogeneous cell distribution and bone volume fraction throughout the cement via the capillarity process mechanism.

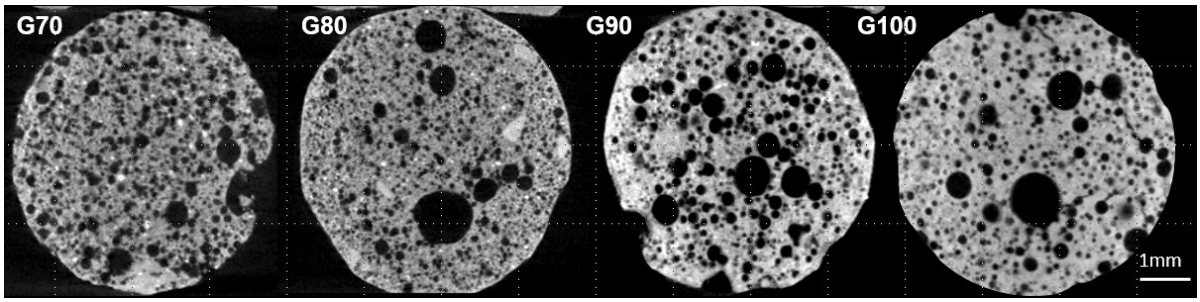

Fig.8 - Micro-CT scanning of the cross sections of the α-TCP foamed cement with different α-TCP /CSH ratios after 24h hardening.

All groups exhibited at least one macropore with a size equal to or greater than 700 μm. There can be two reasons for this: the formation of a larger bubble during the injection of cement into the mold or by a process known as Ostwald´s maturation, which consists of the diffusion-controlled growth process where larger bubbles grow at the expense of shrinking and the eventual disappearance, of smaller bubbles. As a result, the diameter increases and the total number of bubbles decreases [50]. Foam is an unstable thermodynamic system due to its high interfacial area, which considerably increases the free energy of the system. For this reason, after foaming, physical phenomena occur, such as Ostwald's maturation, aiming at reducing free energy and thus destabilizing foam. Therefore, the coalescence of the bubbles, increases depending on the life of the foam. Since it was observed that the experimental cement samples maintained the morphology of the foams, their setting time should influence the pore size. However, in this study, it was not possible to determine the initial setting times by the Gillmore needle method (ASTM C-266-89), because the load attributed to the needles (0.3 and 5MPa) exceeded the compressive strengths of the foamed cements before hardening.

3.3.5 Degradation

Fig. 9 presents the results of sample degradation after 7 and 21 days in SBF. Weight changes are a consequence of the combined variation of (α-TCP and CSH) dissolution and formation of the apatite layer. The results show that the introduction of CSH into CPC can affect the hydration process of CPC and increase the porosity of the internal structure [Tab.2]. According to [43], the mixture of micro nano calcium phosphate and calcium sulfate can effectively improve the degradation rate of bone cement [42]. Traditional CPC usually have low degradation rates and often their weight increases after long periods of immersion as a result of late α-TCP hydrolysis or due to the formation of the apatite layer on the surface of the samples.

Nadkarni [44] also reported that composites of calcium sulphate with calcium phosphate can be formulated to resorb at controlled rates. A composite containing 35% calcium phosphate showed 33.33% resorption after 3 weeks in femoral metaphyseal defects in rabbits. After 6 weeks the resorption was 51.28%. That is to compare with the incorporation of other types of crystals, mannitol and sucrose for

instance, which resorb within 2 days *in vitro,* provoking a serious loss in strength during the first critical days of defect stabilization.

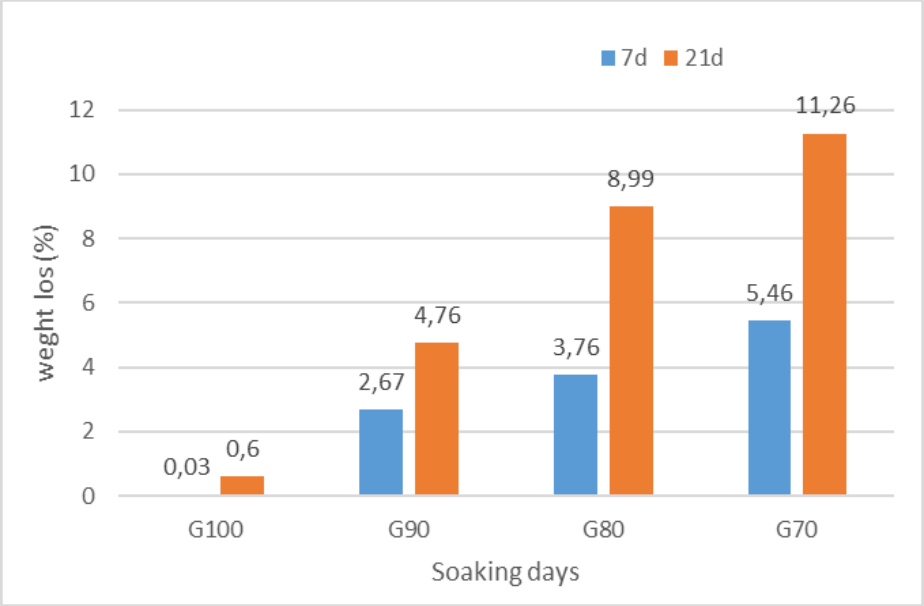

Fig. 9. Degradation rate of CPC groups at 7 and 21 days immersed in SBF.

3.3.6 pH

pH measurements performed in SBF have shown that the pH of the solution decreases with time in all groups. The decrease in the pH value may indicate a gradual dissolution of calcium sulfate during immersion in SBF solution. The decrease was higher in G90 pH decreased (7,02 to 5,7) in 21 days. α-TCP and CDHA have almost the same composition, the setting reaction does not provoke a change of pH, but when CSD and phosphate ions are simultaneously present in the cement, CSD can precipitate with phosphate ions according to reaction: $9CaSO_4 \cdot 2H_2O + 6HPO_4^{2-} \rightarrow Ca_9(PO_4)_5(HPO_4)OH + 6H^+ + 9SO_4^{2-} + 17H_2O$ and release hydronium ions that can lower the pH values, increasing α-TCP solubility. The decrease is stronger for larger CSD and phosphate concentrations [32].

Another reason that the pH solution decreases in the first 24 hours after immersion in SBF may be because α-TCP has a lower Ca/P ratio than HA and, during the dissolution of α-TCP particles, H_3PO_4 formation may occur [51].

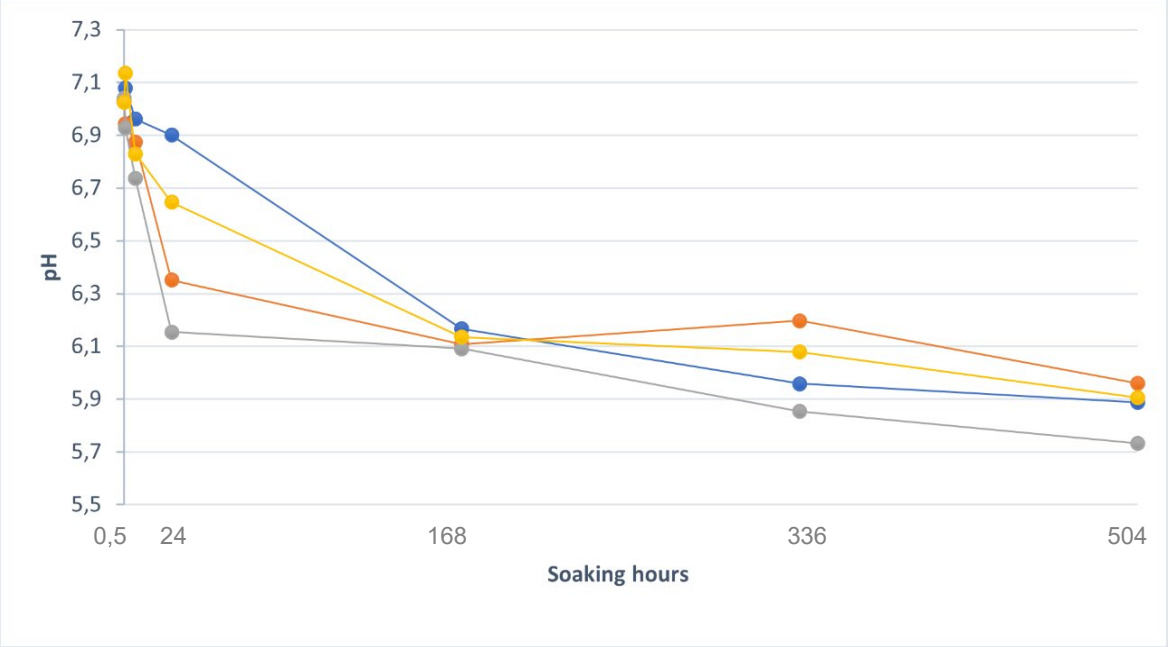

Fig. 10 - pH value of SBF solution for different periods of time wherein hardened cement was immersed.

3.3.7 Morphology (SEM)

SEM analyses revealed the morphology of the cement samples with interconnected pores with varying sizes on the order of macro (>100μm) and microporosity (<100 μm). Many macropores with spherical, distorted shapes and larger sizes were arbitrarily distributed in the foamed cements groups.

Since CDHA is the main product of cement hydration based on α-TCP, it is difficult to predict the ability of this material to induce apatite deposition in SBF. However, the observation of microstructure by SEM is an effective method to estimate the bioactivity of materials, considering that the CDHA crystals deposited from the SBF solution have different microstructure.

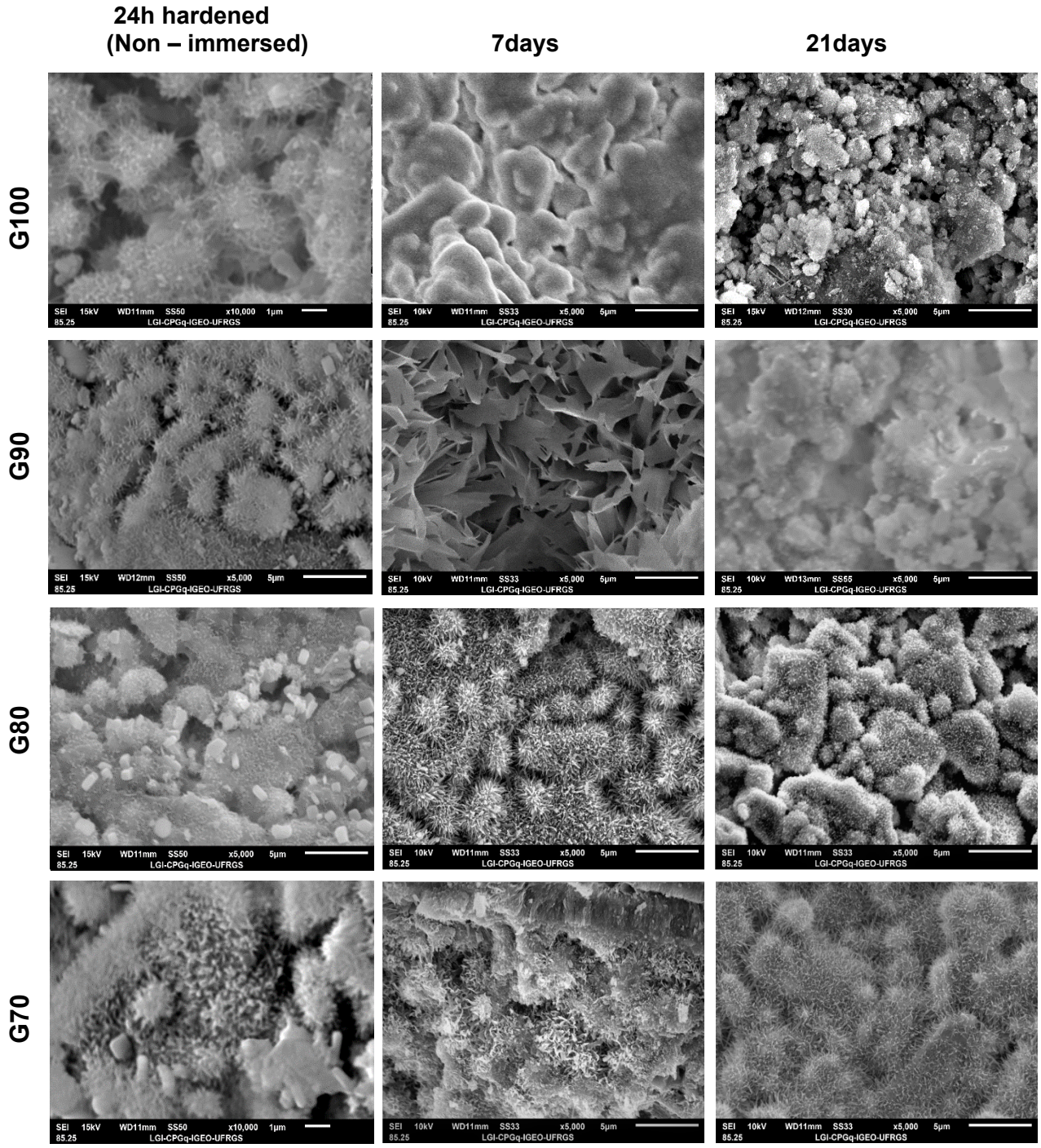

Fig.11 - SEM images show the surface of hardened cements non immersed and immersed in SBF solution for 7 and 21 days. In micrographs, hydroxyapatite needles and petal formation can be observed in all groups in which CSH was present. G90, G80 and G70 21 days immersed, consisted basically in CDHA. The crystals had grown compared to the previous cements and were almost around 2-5 µm. All micrographs at 5000x magnification, except G100 and G70 24h hardened non-immersed micrographs at 10000x magnification.

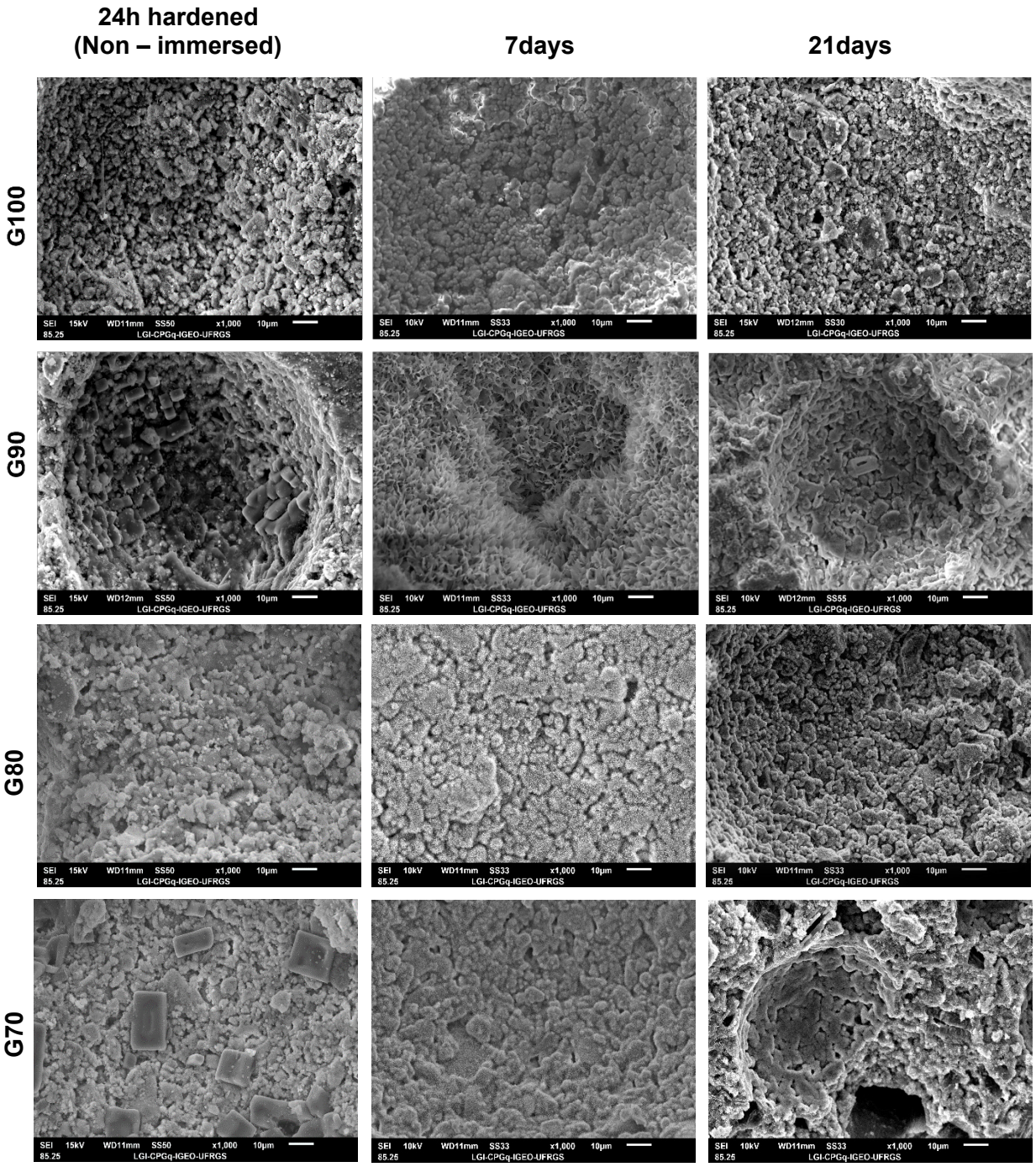

Fig. 12 - SEM images show the surface of hardened cements non immersed and immersed in SBF solution for 7 and 21 days. All micrographs at 1000x magnification.

Figure 11 and 12 show the evolution of the cement surface microstructure during immersion in SBF. The cement consisting only of α-TCP has a thin layer of small CDHA crystals (on the order of 2-3 μm and characterized by growth in form of circles or craters) which are observed deposited on the largest α-TCP grains. At this stage, the smallest α-TCP particles have dissolved and the CDHA layer produces a delay in the hydrolysis reaction [12]. For immersion times, 7 and 21 days, petaloid and rod-shaped crystals are observed. In micrographs G90 (7 days) can be observed clearly, typical petal-like plates of CDHA formation perpendicular to the

α-TCP surface, thus probably minimizing the formation of a diffusion barrier (Hadley´s grain). The decrease in the apparent petal-like plates of all compositions after 21 days of immersion in SBF may be linked to a process of solubilization and reprecipitation of CDHA, which would allow its precipitation in the porosity of the cement and its reduction [51]. Another hypothesis is, with immersion in SBF, the precipitation of small particles of CaP grow in interstices of the surface at the expense of those initially formed, filling the voids in the cement, resulting in greater crystallinity [43].

CSD crystals were small and needle shaped (approx. 10 μm in length) whereas the CSH crystals were large rectangular blocks [52]. G70 non-immersed in SBF shows CSH unreacted crystals. Probably CSH has started to be transformed into smaller CSD crystals, but the hydration reaction has not been accomplished.

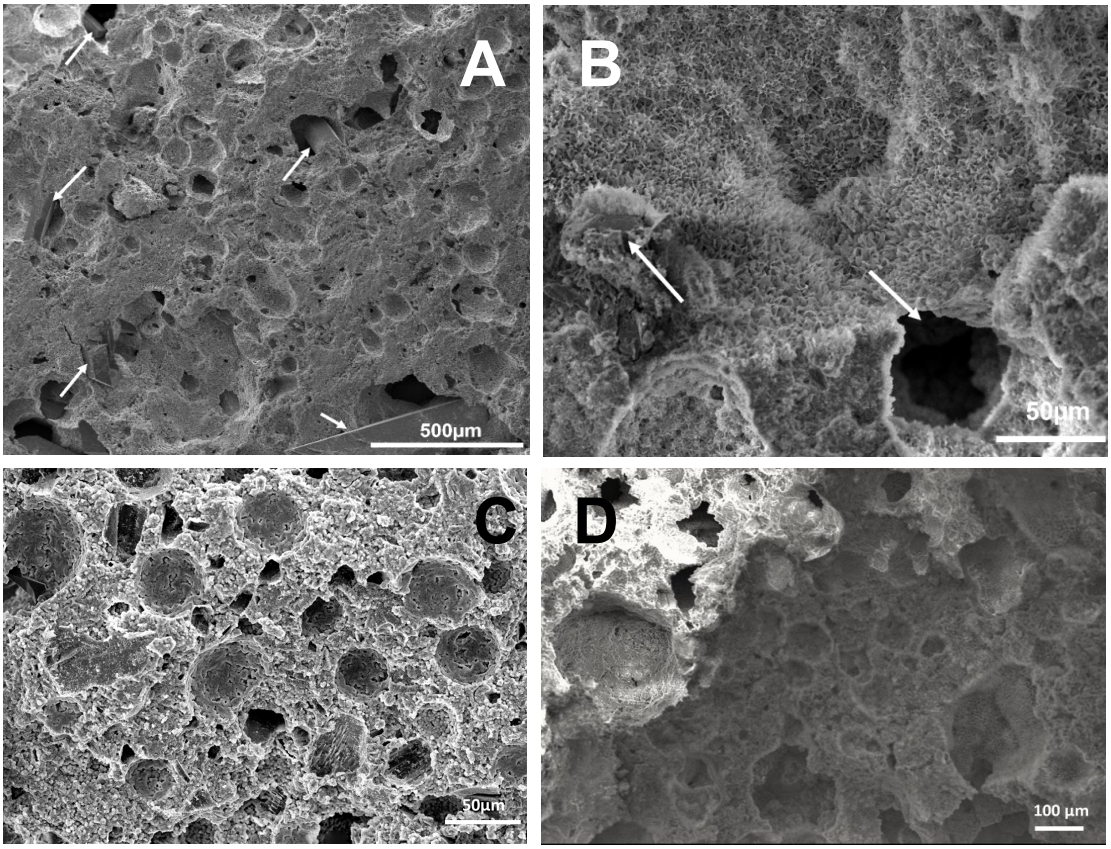

Fig.13 (A) SEM image showed the presence of needle-like CSD crystals embedded in apatitic matrix in G80 (7 days) at 50x magnification. (B) shows G90 (7 days) with α-TCP crystals, on the order of 25 μm, embedded in the CDHA matrix. These crystals were also detected by XRD. The micropore observed, probably was CSD crystals dissolved at (300x magnification). (C) G70 (7 days) at 300x magnification. (D) G90 (7 days) at 100x manification.

Figures 13 (A, C and D) shows several spherical pores proving the effectiness of the present foaming strategy and micro and macropores originating probably from CSD dissolution with the shape of entrapped CSD crystals. Smirnov et al. [27] also observed this porosity with diferent orientations indicating that the cements were well mixed and homogeneously distributed during samples preparation. Nilsson et al. [52] found CSD crystals in samples after 14 days in saline solution where α-TCP was the major phase present. This seems to be related to a blockade effect of CSH hydration because of local pH changes caused by higher concentration of phosphate ions in the solution. Moreover, the formation of a layer of CDHA crystals around the CSH particles renders water diffusion difficult and prevents expansion of CSH. Czechowska et al. [38] related the presence of crystals to the process of dissolution of the CSD surface when in contact with the liquid phase and subsequent reprecipitation of calcium sulfate dihydrate. These dissolution properties may be modified by the presence of ions which adsorb on the surface and hinder the detachment of Ca^{2+} and SO_4^{2-} ions. Phosphate salts are known to play this role for calcium salts for both dissolution and growth [53,54].

Before immersion in SBF, crystals in the form of needles or petals can be observed growing in a tangled network form, characteristic of α-TCP cements [55]. After immersion, the crystals grow in the form of rods in the surface interstices at the expense of those initially formed. After hardening, the petal-shaped crystals precipitate and grow epitaxially, being responsible for the adhesion and cross-linking of the grains.

At the beginning of our study, no evidence was found in the literature of related methods to prepare a foamed injectable cement based on α-TCP, CSH mixed with hidrogen phosphate (Na_2HPO_4), sodium alginate ($C_6H_7NaO_6$) and Lutensol ON 110. Nevertheless, as yet, there is no ideal bone cement. Each material must be used based on its characteristics and with knowledge of its limitations.

3.4 Conclusion

In the present study, a simple method was developed to prepare a foamed injectable cement based on α-TCP and CSH. The results indicated that the foamed cement have excelente injectability, heterogeneous interconnected porosity achieved by foaming process and CSD dissolution. Biphasic cements (α-TCP/CSH) showed to be more bioactive than α-TCP alone, showing desirable and promising characteristics for bone tissue regeneration. Probably some adjustments in the formulation of our foamed cements will improve their mechanical performance, and interconnected macroporosity, increasing their potential use. Further studies are necessary to confirm our findings and *in vivo* studies are essential to evaluate the application of the foamed cements developed in this study.

References

[1] Şahin E. Calcium Phosphate Bone Cements. In: Saleh HEM., Rahman ROA editors. Cement Based Materials [Internet]. London: IntechOpen; 2018 [cited 2022 May 10]. Available from: https://www.intechopen.com/chapters/61543 doi: 10.5772/intechopen.74607

[2] Ginebra C, Canal M, Espanol D, Pastorino EB. Montufar Calcium phosphate cements as drug delivery materials Adv. Drug Deliv. Na., 2012;64:1090-1110, http://dx.doi.org/10.1016/j.addr.2012.01.008

[3] Montufar EB, Maazouz Y, Ginebra MP, Relevance of the setting reaction to the injectability of tricalcium phosphate pastes, Acta Biomater., 2013;9:6188–6198, http://dx.doi.org/10.1016/j.actbio.2012.11.028.

[4] Heinemann S., Rössler M., Lemm M. Ruhnow B., Nies. Properties of injectable ready-to-use calcium phosphate cement based on water-immiscible liquid, Acta Biomater., 2013;9:6199–6207 http://dx.doi.org/10.1016/j.actbio.2012.12.017

[5] LeGeros RZ, Chohayeb A, Shulman A. Journal of Dental Research, 1982;61:343.

[6] Brown L, Chow A. new calcium phosphate setting cement. J. Dent. Res., 1983;62:672–679.

[7] Habraken W, Habibovic P, Epple M, Bohner M. Calcium phosphates in bio-medical applications: materials for the future? Mater. Today, 2016;19(2):69–87.

[8] Ginebra MP, Espanol M, Montufar EB, Perez RA. Mestres, G. New processing approaches in calcium phosphate cements and their applications in regenerative medicine. Acta Biomaterialia, 2010; 6(8):2863–2873

[9] Yuan Y, Li J.D. de Bruijn et al. Tissue responses of calcium phosphate cement: a study in dogs. Biomaterials, 2000;21:1283–1290.

[10] LeGeros RZ. Calcium phosphate-based osteoinductive materials. Chem Na, 2008;1084742–4753.

[11] Ginebra M, Espanol Y, Maazouz V, Bergez D. Pastorino. Bioceramics and bone healing. EFORT Open Na., 2018;5:173-183 doi:10.1302/2058-5241.3.170056.

[12] Ginebra M, Driessens F, Planell J. Effect of the particle size on the micro and nanostructural features of a calcium phosphate cement: a kinetic analysis, Biomaterials, 2004;25(17):3453–3462.

[13] Ginebra M, Driessens F, Planell J., Fernández E. Driessens, J.A. Planell, Modeling of the Hydrolysis of α-Tricalcium Phosphate, Journal of the American Ceramic Society, 1999;82(10):2808–2812.

[14] Seebach C, Schultheiss J, Wilhem K, Frank J, Henrich D. Comparison of six bone-graft substitutes regarding to cell seeding efficiency, □oné□te□nte and growth behavior of human mesenchymal stem cells (MSC) in vitro. International Journal of the Care of the Injured., 2010;41:731-8.

[15] Shayegan A, Petein M, Abbeele AV. Beta-tricalcium phosphate, □oné□ mineral trioxide aggregate, □oné□ Portland cement, ferric sulfate, and formocresol used as pulpotomy □oné□te in primary pig teeth. Oral Surgery,Oral Medicine, Oral Patho-logy, Oral Radiology & Endodontics., 2008;105:536-42.

[16] Hankermeyer KL, Ohashi DC, Delaney J, Ross BR. Constantz. Dissolution rates of carbonated hydroxyapatite in hydrochloric acid. Biomaterials 2002;23:743–50

[17] Almirall A, Larrecq G, Delgado JA, Martínez S, Planell JA, Ginebra MP. Fabrication of low temperature macroporous hydroxyapatite scaffolds by foaming and hydrolysis of an a- TCP paste. Biomaterials, 2004;25:3671–80.

[18] Sarda S, Fernandez E, Nilsson M, Planell JA. Influence of surfactant molecules as air-entraining agent on bone cement macroporosity. J Biomed Mater Res, 2003;65A:215–21.

[19] Del Real RP, Wolke JGC, Vallet-Regı M, Jansen JA. A new method to produce macropores in calcium phosphate cements. Biomaterials, 2002;23:3673–80.

[20] Thomas, DA. Puleo. Calcium sulfate: Properties and clinical applications. J Biomed Mater Res Part B 88B;2008:597-610.

[21] Shams M, Nezafati N, Poormoghadam D, Zavareh S, Zamanian A, Salimi A. Synthesis and characterization of electrospun bioactive glass nanofibers-reinforced calcium sulfate bone cement and its cell biological response, Ceram. Int., 2020;46:10029–10039.

[22] Bahn SL. Plaster: a bone substitute, oral surgery, oral medicine, Oral Pathology, 1966;21:672–681.

[23] Carlson M, Nilsson E, Fernandez JA. Planell, An ultrasonic pulse-echo technique for monitoring the setting of CaSO4-based bone cement, Biomaterials, 2003;24(1):71–77 https://doi.org/10.1016/s0142-9612(02)00253-3.

[24] Wang MI, Chen W, Niu DD, Winston W, Cheng BO. Lei, Injectable biodegradation-visual self-healing citrate hydrogel with high tissue penetration for microenvironment-responsive degradation and local tumor therapy, Biomaterials, 2020;261:120301, https://doi.org/10.1016/j.biomaterials.2020.120301.

[25] Mingzu Q, Li J, Chen K. Liu Design and characterization of injectable abalone shell/calcium sulfate bone cement scaffold for bone defect repair. Chemical Engineering J, 2021;420:129866 https://doi.org/10.1016/j. cej.2021.129866

[26] Demir-Oğuz AR, Boccaccini D. Loca. Injectable bone cements: What benefits the combination of calcium phosphates and bioactive glasses could bring? Bioactive Materials, 2023;19:217 – 236 https://doi.org/10. 1016/j.bioactmat. 2022.04.007

[27] Smirnov VV, Khairutdinova DR, Antonova OS, Goldberg MA, Smirnov SV, Barinov SM. Composite Cement Materials Based on Calcium Sulfate and Phosphate for Medicine. Chemical Technology., 2018;483:279–282 DOI: 10.1134/S0012500818110083

[28] Du MZ, Li Q, Chen K, Liu H, Song C. Design and characterization of injectable abalone shell/calcium sulfate bone cement scaffold for bone defect repair, Chem. Eng. J., 2021;420:129866

[29] Vásquez S, Domínguez S, Santos LAL. α-TCP cements prepared by syringe-foaming: Influence of Na_2HPO_4 and surfactant concentration. Mater Sci Eng C Mater Biol Appl., 2017;81(1):148-155. Doi: 10.10s16/j.msec.2017.07.056. Epub 2017 Aug 1. PMID: 28887959.

[30] Kokubo T, Takadama H. How useful is SBF in predicting in vivo bone bioactivity? Biomaterials, 2006;27:2907–2915 doi: 10.1016/j.biom-aterials.2006.01.017

[31] Vasquez AF. Obtenção e caracterização de cimentos macroporosos de α-Tcp pelo método de espumação direta manual. 2016. 117p. Dissertação (Mestrado em Engenharia de Minas, Metalúrgica e Materiais) Universidade Federal do Rio Grande do Sul. Porto Alegre. 2016

[32] Bohner M. New hydraulic cements based on alpha-tricalcium phosphate-calcium sulfate dihydrate mixtures. Biomaterials. 2004;25(4):741-749. Doi:10.1016/s 0142-9612(03)00573-8

[33] Carrodeguas S. De Aza α-Tricalcium phosphate: synthesis, properties and biomedical applications. Acta Biomater. 2011;10:3536-3546. Doi:10.1016/ j.actbio.2011.06.019

[34] Prasad et al. Indian J. Dairy Sci., 2005;58 (2):109-112

[35] Bensted J, Prakash S. Investigation of the Calcium Sulphate-Water System by Infrared Spectroscopy. Nature, 1968; 219,60–61. https://doi.org/10. 1038/ 219060a0

[36] Putnis A, Winkler B, Fernandez-Diaz L. In situ IR spectroscopic and thermogravimetric study of the dehydration of gypsum. Mineralogical Magazine, 1990;54(374):123-128. Doi:10.1180/minmag.1990.054.374.14

[37] Manoj et al. Manoj B. Synthesis and characterization of porous, mixed phase, wrinkled, few layer graphene like nanocarbon from charcoal. Russ J Phys Chem A2, 015;89(13):2438–2442

[38] Czechowska J, Zima A., Ślósarczyk A. Comparative study on physicochemical propertiesof alpha-TCP / calcium □oné□te dihydrate biomicroconcretes containing chitosan, sodium alginate or methylcellulose *A*cta of Bioengineering and Biomechanics 2020;22(1) DOI: 10.37190/ABB-01458-2019-02

[39] Toyama T, Kameda S, Nishimiya N. Synthesis of Sulfateion – substituted Hydroxyapatite from Amorphous Calcium Phosphate, Bioceram. Dev. Appl., 2013;S1: 011, DOI:10.4172/2090-5025.S1-011.

[40] Montufar EB, Traykova T, Gil C, et al. Foamed surfactant solution as a template for self-setting injectable hydroxyapatite scaffolds for bone regeneration. Acta Biomater. 2010;6(3):876-885. doi:10.1016/j.actbio.2009.10.018

[41] Zhang J, Liu W, Gauthier O. et al. A simple and effective approach to prepare injectable macroporous calcium phosphate cement for bone repair: Syringe-foaming using a viscous hydrophilic polymeric solution. Acta Biomaterialia. 2016;31:326-338. https://doi.org/10.1016/j.actbio.2015.11.055

[42] Almirall A, Larrecq G, Delgado J, Martinez S, Planell J, Ginebra M. Fabrication of low temperature macroporous hydroxyapatite scaffolds by foaming and hydrolysis of na α-TCP paste. Biomaterials. 2004;17(25):3671–3680.

[43] Cai Z, Zhiwen W, Yi W, Tao Y, Changren Zhou Manipulation of the degradation behavior of calcium phosphate and calcium sulfate bone cement system by the addition of micro-nano calcium phosphate 2021 https://doi.org/10.1016/j. ceramint.2021.07.08

[44] Nadkarni PP, Ricci JL, Parsons JR, Hawkins M, Dimaano F, Patel D, Tarkin I, Garcia J. An in vivo evaluation of calcium sulfate composite graft materials using rabbit metaphyseal and calvarial defect. In: von Recum AF, Lucas LC. Sixth World Biomaterials Congress Transactions, vol. I. Minneapolis: Society for Biomaterials; 2000:113.

[45] Abbasi A, Hamlet S, Love RM, Nguyen NT. Porous scaffolds for bone regeneration. Journal of Science: Advanced Materials and Devices. 2020;5(1):1-9 https://doi.org/10.1016/j.jsamd.2020.01.007.

[46] Morejon JA, Delgado AA, Ribeiro MVO, Mendizabal E, Garcia I, Alfonso A, Poh P, Griensven M, Balmayor ER. Development, characterization and in vitro biological properties of scaffolds fabricated from calcium phosphate nanoparticles], Int. J. Mol. Sci. 2019;20(7). https:// doi.org/10.3390/ijms20071790

[47] Murphy, C.M, Haugh, M.G., O'Brien, F.J. The effect of mean pore size on cell attachment, proliferation and migration in collagen-glycosaminoglycan scaffolds for bone tissue engineering, Biomaterials. 2010; 31 (3) :461-466, https://doi.org/10.1016/j.biomaterials.2009.09.063.

[48] Murphy CM, O'Brien FJ. Understanding the effect of mean pore size on cell activity in collagen-glycosaminoglycan scaffolds, Cell Adhes. Migrat. 2010;4(3):377e381, https://doi.org/10.4161/cam.4.3.11747.

[49] Rustom TB, Loub S, Pignot-Paintrand I, Nemkee BW, Lue Y, Mark M, Catherine P, Johnsona AJW, Micropore-induced Capillarity Enhances Bone Distribution in vivo in Biphasic Calcium Phosphate Scaffolds Acta Biomater. 2016 October 15; 44: 144–154. Doi:10.1016/j.actbio.2016.08.025.

[50] Rocha CM. Evolução de bolhas de ar em misturas de glicerol/água pelo amadurecimento de Ostwald. 2018. 85 f. Dissertação (Mestrado em Física Aplicada) – Universidade Federal de Viçosa, Viçosa. 2018.

[51] Santos LA. Dos. Desenvolvimento de cimento de fosfato de cálcio reforçado por fibras para uso na área médico-odontológica. Tese de Doutorado. Unicamp. Brasil, 2002

[52] Nilsson E, Fernández S, Sarda L, Lidgren JA. Planell Characterization of a novel calcium phosphate/sulfate bone cement J Biomed Mater Res, 2002;61: 600–607.

[53] Liu ST, Nancollas GH. The crystal growth of calcium sulfate dihydrate in the presence of additives, J. Colloid Interface Sci., 1973;44(3):422–429.

[54] Pachon-Rodriguez EA, Colombani J. Pure dissolution kinetics of anhydrite and gypsum in inhibiting aqueous salt solutions, AIChE. J., 2013;59(5):1622–1626.

[55] Driessens FCM, Fernandez E, Ginebra MP, Boltong MG, Planell JA. Calcium phosphates and ceramic bone cements vs. acrylic cements. Anal Quim Int Ed, 1997;93:38–43.

4 CONSIDERAÇÕES FINAIS

O ajuste da taxa de degradação para corresponder à cinética da formação óssea ainda é um grande desafio para a engenharia tecidual e para a ciência dos biomateriais.

Ajustar as concentrações de aditivos como agentes espumantes ou porogênicos na produção e estabilidade de espumas são sugestões para trabalhos futuros. Segundo Torres e colaboradores (2015) CPCs sem aditivos não possuem boa coesão e tendem a desintegrar quando em contato com fluidos corporais no leito cirúrgico.

Aumentar a viscosidade do CPC adicionando à fase líquida biopolímeros naturais como sulfato de condroitina (Shi et al., 2018), microesferas de gelatina (NEZAFATI et al., 2019), poliacrilato de sódio ou hydrogel de PLGA-PEG-PLGA (XIE, et al., 2020), polímero fluido à temperatura ambiente que se converte em gel-viscoso à temperature corporal, melhoraria a coesão do CPC.

Combinar CPC injetável em forma de espuma e células vivas encapsuladas *in vitro*, antes do aprisionamento no CPC, pode ser uma alternativa promissora para regeneração óssea em cirurgias minimamente invasivas. Zhao et al. (2010) desenvolveram CPCs injetáveis com células-tronco mesenquimais derivadas de cordão umbilical humano, WANG et a. (2016) e TAO et al. (2018), derivadas da medula óssea. Todos os resultados mostraram que as fontes celulares e os novos CPCs injetáveis com células encapsuladas eram promissoras para engenharia óssea.

É provável que com ajustes na formulação que melhorem o desempenho mecânico, reforcem a coesão e aumentem a macroporosidade interconectada, este CPC injetável, em forma de espuma, possa ser impresso para fabricação de modelos tridimensionais de suportes porosos para regeneração óssea (robocasting).

REFERÊNCIAS

ABBASI, A.; HAMLET, S.; LOVE, R.M.; NGUYEN, N.T Porous scaffolds for bone regeneration. **Journal of Science: Advanced Materials and Devices**. v.5, n.1, p.1-9, 2020 https://doi.org/10.1016/j.jsamd.2020.01.007.

AGHDASI, B.; MONTGOMERY, S.R.; DAUBS, M.D.; WANG, J.C. A review of demineralized bone matrices for spinal fusion: The evidence for efficacy. **The Surgeon.** Disponível em: https://doi.org/10.1016/j.surge.2012.08.001

ALMIRALL, A.; LARRECQ, G.; DELGADO, J.; MARTINEZ, S.; PLANELL, J.; GINEBRA, M. Fabrication of low temperature macroporous hydroxyapatite scaffolds by foaming and hydrolysis of an α-TCP paste. **Biomaterials.** v.17, n.25, p.3671–3680, 2004.

ALVES, H.L.R. **Cimento de fosfato tricálcio: síntese e influência de aditivos na sua injetabilidade.** 2005. 106p. Dissertação de Mestrado. Universidade Federal do Rio Grande do Sul. Programa de Pós-Graduação em Engenharia de Minas, Metalúrgica e Materiais. Porto Alegre, 2005.

AMBARD, A.; MUENINGHOFF, L. Calcium Phosphate Cement: Review of mechanical and biological properties. **Journal of Prosthodontics**, v. 15, p.321-328, 2006.

BOCCACCIO, A.; UVA, A.E.; FIORENTINO, M.; MORI, G.; MONNO, G. Geometry design optimization of functionally graded scaffolds for bone tissue engineering: a mechanobiological approach, **PloS One**, v.11 n.11, 2016. https://doi.org/ 10.1371/journal.pone.0146935.

BIGI A.; BRACCI, B.; PANZAVOLTA, S. Effect of added gelatin on the properties of calcium phosphate cement. **Biomaterials,** v.25, p.2893–9, 2004.

BOHNER, M. Resorbable biomaterials as bone graft substitutes. **Mater. Today**. v.13, n1-2, p. 24-30, 2010. https://doi.org/10.1016/S1369-7021(10)70014-6

BOHNER, M.; DOBELIN, N.; BAROUD, G. Theoretical and experimental approach to test the cohesion of calcium phosphatepastes. **European Cells & Materials**, v.12, p.26–35, 2006.

BOHNER, M.; BAROUD, G. Injectability of calcium phosphate pastes. **Biomaterials.** v.26, p. 1553-63, 2005 doi: 10.1016/j.biomaterials.2004.05.010. PMID: 15522757.

BOHNER, M. Calcium orthophosphates in medicine: from ceramics to calcium phosphate cements, **Injury**, v.31, p. 37-47, 2000.

BROWN, L.; CHOW. A new calcium phosphate setting cement, **J. Dent. Res.** v.62, p. 672–679, 1983.

BUSER, D. **Vinte Anos de Regeneração óssea guiada na implantodontia**. São Paulo: Santos, p. 256, 2010.

CAMIRÉ, CL; SAINT-JEAN, S.J; HANSEN, S; MCCARTHY, I; LIDGREN, L. Hydration Characteristics of α-tricalcium Phosphates: Comparison of Preparation Routes. **Journal of Applied Biomaterials and Biomechanics**. v. 2, n.3, p.106-111, 2005. doi:10.1177/228080000500300205

CANAL, C; GINEBRA, M.P. Fibre-reinforced calcium phosphate cements: a review. **J Mech Behav Biomed Mater** v.4, p.1658-1671, 2011.

CHEN, W. W.; THEIN-HAN, M.D.; WEIR, Q.; CHEN, H.H.; XU. Prevascularization of biofunctional calcium phosphate cement for dental and craniofacial repairs, Dental Materials:official publication of the **Academy of Dental Materials**. v.30, n.5, p. 535–544, 2014.

DOROZHKIN S.V. Functionalized calcium orthophosphate and their biomedical applications **J. Mater. Chem. B**, v.7, p.7471-7489, 2019. https://doi.org/10.1039/C9TB01976F

DOROZHKIN S.V. Self-setting calcium orthophosphate ($CaPO_4$) formulations. In: **Developments and Applications of Calcium Phosphate Bone Cements**. Singapore: Springer; p. 141-146, 2018 DOI:10.1007/978-981-10-5975-9

DOROZHKIN S.V. Calcium Orthophosphate-Based Bioceramics. **Materials** (Basel, Switzerland), v.9, n.6, p. 3840–3942, 2013. https://doi.org/10.3390/ma6093840

DOROZHKIN, S. V. Calcium Orthophosphates in Nature. **Biology and Medicine Materials,** v.2, p.399-498, 2009. Disponível em: https://doi.org/10.3390/ma2020399

DOROZHKIN, S. V. Calcium orthophosphates. **Journal of Materials Science: Materials in Medicine**, v.42, p.1061–1095, 2007.

ELIAZ, N.; METOKI, N. Calcium phosphate bioceramics: A review of their history, structure, properties, coating technologies and biomedical applications. **Materials** v.10, p.334, 2017.

FERNANDEZ-YAGUE, M.A, ABBAH S.A, MCNAMARA L, ZEUGOLIS D.I, PANDIT A, BIGGS M.J. Biomimetic approaches in bone tissue engineering: Integrating biological and physicomechanical strategies. **Adv Drug Deliv Rev**. v.84, p. 1-29, 2015 doi:10.1016/j.addr.2014.09.005

GINEBRA, MP; ESPANOL, M; MAAZOUZ, Y; BERGEZ, V; PASTORINO, D. Bioceramics and bone healing. **EFORT Open Rev**. v.5, n.3, p. 173-183, 2018. doi:10.1302/2058-5241.3.170056

GINEBRA, M. P.; ESPANOL, M.; MONTUFAR, E. B.; PEREZ, R. A.; MESTRES, G. New processing approaches in calcium phosphate cements and their applications in regenerative medicine. **Acta Biomaterialia**, v.6, n.8, p. 2863–2873, 2010.

GINEBRA, M.P.; DRIESSENS,F.; PLANELL, J. Effect of the particle size on the micro and nanostructural features of a calcium phosphate cement: a kinetic analysis, **Biomaterials,** v.25, n.17, p. 3453–3462, 2004.

GINEBRA, M.P.; FERNANDEZ, F.C.; DE MAEYER, E.; VERBEEK, R.M.; BOLTONG, M.G.; GINEBRA, J.; PLANELL, J.A. Setting reaction and hardening of an apatitic calcium phosphate cement. **Journal of Dental Research**, v.76, p.905-912, 1997.

GRAZIANI, G.; BOI, M.; BIANCHI, M. A review on ionic substitutions in hydroxyapatite thin films: Towards complete biomimetism. **Coatings**, v.8, p. 269, 2018.

HABRAKEN, W.J; HABIBOVIC, P.; EPPLE, M.; BOHNER, M. Calcium phosphates in biomedical applications: materials for the future? **Mater. Today** v.2, n.19, p. 69-87, 2016.

HABRAKEN, W.; WOLKE, J; MIKOS, A.; JANSEN, J.A. PLGA microsphere/calcium phosphate cement composites for tissue engineering: in vitro release and degradation characteristics **J. Biomater. Sci. Polym**. v.19, p.1171–88, 2008.

HABRAKEN, W.J.; WOLKE, J.G.; JANSEN, J.A. Ceramic composites as matrices and scaffolds for drug delivery in tissue engineering, **Advanced drug delivery reviews,** v.59 n. 4-5, p. 234–24, 2007.

HADLEY, D. W. DOLCH, W. L.; DIAMOND, S. On the occurrence of hollow-shell hydration grains in hydrated cement paste**. Cement and Concrete Research**, v.30, p.1–6, 2000.

HANDA, T.; ANADA, T.; HONDA, Y.; YAMAZAKI, H.; KOBAYASHI, K.; KANDA, N.; KAMAKURA, S.; ECHIGO, S.; SUZUKI, O. The effect of na octacalcium phophate co-precipitated gelatina composite on the repair of critical-sized rat calvarial defects. **Acta Biomaterialia**, v.8, p.1190-1200, 2012.

HANKERMEYER, CR; OHASHI, KL; DELANEY, DC; ROSS, J; CONSTANTZ, BR. Taxas de dissolução de hidroxiapatita carbonada em ácido hidro-clorado. **Biomateriais**, v.23, p.743-50, 2002.

HAUGEN, J.H.; LYNGSTADASS, S.P.; ROSSI, F.; PERALE, G. Bone grafts: which is the ideal biomaterial? **J Clin Periodontol**., v.11, n.1, 2019. DOI: 10.1111/jcpe.13058

HAY, I. D. et al. Bacterial biosynthesis of alginates. **J. Chem. Technol. Biotechnol**., v.85, p.752–759, 2010.

HOPPE, A.; GÜLDAL, N.S.; BOCCACCINI, A.R. A review of the biological response to ionic dissolution products from bioactive glasses and glass-ceramics. **Biomaterials**, v.32, n.11, p.2757-74, Apr 2011 https://doi.org/10. 1016/j.biomaterials. 2011.01.004.

HUSE, R.O.; RUHE, P.Q.; WOLKE, J.G.; JANSEN, A. The use of porous calcium phosphate scaffolds with transforming growth factor beta 1 as an onlay bone graft substitute. **Clin Oral Implants Res**, v.6, n.15, p.741–749, 2004.

JANSEN, J.A.; VEHOF, J.W.; RUHE, P.Q.; KROEZE-DEUTMAN, H. et al. Growth factor-loaded scaffolds for bone engineering. **Journal of controlled release: official journal of the Controlled Release Society**, v.101 n.1-3, p.127–136, 2005.

JEONG, J.; KIM, J.H.; SHIM, J.H. et al. Bioactive calcium phosphate materials and applications in bone regeneration. **Biomater Res,** v.23, n.4 2019. https://doi.org/10.1186/s40824-018-0149-3

KHAIROUN, I.; BOLTONG, M. G.; DRIESSENS, F. C. M.; PLANELL, J. A. Limited compliance of some apatitic calcium phosphate bone cements with clinical requirements. **Journal of Materials Science: Materials in Medicine**, v.11, n.9, p. 667–671, 1998.

KROESE-DEUTMAN, H.C.; RUHE, P.Q.; SPAUWEN, P.H.; JANSEN, J.A. Bone inductiveproperties of rhBMP-2 loaded porous calcium phosphate cement implants inserted at an ectopic site in rabbits, **Biomaterials** v.26, n.10, p.1131–1138, 2005.

KUCKO, N.W.; HERBER, R.-P.; LEEUWENBURGH, S.C.G.; JANSEN, J.A. Calcium Phosphate Bioceramics and Cements. In **Principles of Regenerative Medicine;** Elsevier: Amsterdam, The Netherlands, p. 591–611, 2019

LANAO, R. P. F; LEEUWENBURGH, S. C; WOLKE, J. G.; JANSEN J. A. Bone response to fast-degrading, injectable calcium phosphate cements containing PLGA microparticles. **Biomaterials** v.32, p. 8839–47, 2011.

LEGEROS, R.Z. Properties of osteoconductive biomaterials: calcium phosphates, **Clinical orthopaedics and related research** v.395, p81-98, 2002

LEGEROS, R.Z.; COHAYEB, A.; SHULMAN, A. Apatitic calcium phosphates: Possible dental restorative materials. **J Dent Res**., v.61, p.343, 1982.

LI, Y.; JIANG, T.; ZHENG, L.; ZHAO, J. Osteogenic differentiation of mesenchymal stem cells (MSCs) induced by three calcium phosphate ceramic (CaP) powders: A comparative study [published correction appears in **Mater Sci Eng C Mater Biol Appl**. 2020 Jul;112:110867]. **Mater Sci Eng C Mater Biol Appl**. v.80, p. 296-300, 2017. doi:10.1016/j.msec.2017.05.145

LIVINGSTON, T.; DUCHEYNE, P.; GARINO, J. In vivo evaluation of a bioactive scaffold for bone tissue engineering. **Journal of biomedical materials research** v.62, n.1, p. 1-13, 2002.

LIU, W; ZHANG, J; WEISS, P; TANCRET, F; BOULER, JM. The influence of different cellulose ethers on both the handling and mechanical properties of calcium phosphate cements for bone substitution. **Acta Biomater**. v.3, n.9, p. 5740-5750, 2013 doi:10.1016/j.actbio.2012.11.020

LIU, J. et al. The effect of synthetic α-tricalcium phosphate on osteogenic differentiation of rat bone mesenchymal stem cells. American. **Journal of Translational Research**, v. 7, n. 9, p. 588-601, 2015.

LODOSO-TORRECILLA I.; VAN DEN BEUCKEN J.J.J.P.; JANSEN, J.A. Calcium phosphate cements: Optimization toward biodegradability. **Acta Biomater**. v. 119, n.1, p. 1-12, 2021. https://doi.org/10.1016/j.actbio.2020.10.013

LODOSO-TORRECILLA I.; VAN GESTEL, N.A.P.; DIAZ-GOMES, L.; GROSFELD, E.C.Multimodal pore formation in calcium phosphate cements **Journal of Biomedical Materials Research** Part A v.2, n.106, p.500-509, 2018.

LOBO, S.E.; LIVINGSTON ARINZEH, T. Biphasic Calcium Phosphate Ceramics for Bone Regeneration and Tissue Engineering Applications. **Materials,** v.3, p. 815–826, 2010.

LU, J.; YU, H.; CHEN, C. Biological properties of calcium phosphate biomaterials for bone repair: a review. **RSC Advances**, v.8, n.4, July 2018.

MAJI, K.; MONDAL, S. Calcium Phosphate Biomaterials for Bone Tissue Engineering: Properties and Relevance in Bone Repair. In Racing for the Surface: Antimicrobial and Interface. **Tissue Engineering**; Springer: Berlin/Heidelberg, Germany. p. 535–555, 2020.

MONMA, H.; KANAZAWA, T. The hydration of α-tricalcium phosphate. **Yogyo-Kyokai-Shi**, v.84, p. 209–213, 1976.

MONTOYA, C.; DU, Y.; GIANFORCARO, A.L. *et al.* On the road to smart biomaterials for bone research: definitions, concepts, advances, and outlook. **Bone Res,** v.9, n.12, 2021. https://doi.org/10.1038/s41413-020-00131-z

NEZAFATI, N.; FAROKHI, M.; HEYDARI, M.; HESARAKI, S.; NASAB, N.A. In vitro bioactivity and cytocompatablity of an injectable calcium phosphate cement/silanated gelatin microsphere composite bone cement. **Compos. B Eng**. p.175, 2019.

O'NEILL, R.; MCCARTHY, H.O.; MONTUFAR, E.B; GINEBRA, M.P; WILSON, D.I.; LENNON, A.; DUNNE, N. Critical review: injectability of calcium phosphate pastes and cements. **Acta Biomater**. v.50, p.1-19, 2017.

ORÉFICE, R. L.; PEREIRA, M. M.; MANSUR, H. S. **Biomateriais: fundamentos e aplicações.** Cultura Médica: Rio de Janeiro, 2012.

RAMIREZ, C.S.S.; FERRI-ANGULO, D.; DEBRET, R.; GRANIER, F.; MARIE, S.; LEF`EVRE, F.; BOULER, J.M.; DESPAS, C.; SOHIER, J.; BUJOLI, B. Combination of biocompatible hydrogel precursors to apatitic calcium phosphate cements (CPCs): influence of the *in situ* hydrogel reticulation on the CPC properties, J**. Biomed. Mater. Res. B Appl. Biomater.** v.109, p. 102-116, 2021 https://doi.org/10.1002/

RAGHOEBAR, G. M. et al. Long-term effectiveness of maxillary sinus floor augmentation: A systematic review and meta-analysis. **Journal of clinical periodontology**, v. 46, n. 2, p. 307–318, jun. 2019. https://doi.org/10.1111/jcpe.13055

RAMALHO, A. C. A. **Desenvolvimento e caracterização de cimentos ósseos inovadores**, 2010. 101f. Dissertação (Mestrado) - Ciências Biomédicas, Faculdade das Ciências da Saúde, Universidade da Beira Interior, 2010.

REAL, R.P.; OOMS, E.; WOLKE, J.G.; VALLET-REGI, M.; JANSEN, J.A. In vivo bone re-sponse to porous calcium phosphate cement, J**ournal of biomedical materials research.** PartA v.65, n.1, p.30–36, 2003.

REAL, R.P.; WOLKE, J.G.; VALLET-REGI, M.; JANSEN, J.A. A new method to produce macropores in calcium phosphate cements, **Biomaterials** v.23, n.17, p.3673-3680, 2002.

ŞAHIN, E. In book: **Cement Based Materials Chapter**: Rheological characterization of the viscoelastic behavior of calcium phosphate suspensions Synthesis and Characterization of Calcium Phosphate Cement Based Macroporous. October 2018 Scaffolds DOI: 10.5772/intechopen.74607

SANTOS, L. A. Natural Polymeric Biomaterials: Processing and Properties. Reference Module in **Materials Science and Materials Engineering,** Elsevier, 2017. L.A.L. https://doi.org/10.1016/B978-0-12-803581-8.0225

SANTOS, L.A; CARRODÉGUAS, Raúl Garcia; BOSCHI, Anselmo Ortega; ARRUDA, A. C. F. Fiber-Enriched Double Setting Calcium Phosphate Bone Cement. **Journal of Biomedical Materials Research**. Part A, Estados Unidos, v. 65A, n.2, p. 244-250, 2003.

SAKKAS, A.; WILDE, F.; HEUFELDER, M. et al. Autogenous bone grafts in oral implantology—is it still a “gold standard”? A consecutive review of 279 patients with 456 clinical procedures. **Int J Implant Dent** v. 23, n. 3, 2017. https://doi.org/10.1186/s40729-017-0084-4

SCHRÖTER, L.; KAISER, F.; STEIN, S.; GBURECK, U.; IGNATIUS, A. Biological and mechanical performance and degradation characteristics of calcium phosphate cements in large animals and humans, **Acta Biomaterialia**, v.117, p. 1-20, 2020. https://doi.org/10.1016/j.actbio.2020.09.031

SHI, H.; ZHANG, W.; LIU, X.; ZENG, S.; YU, T.; ZHOU, C.I. Synergistic effects of citric acid - sodium alginate on physicochemical properties of α-tricalcium phosphate bone cement. **Ceram. Int.,** v. 45, p. 2146-52, 2019. doi.org/10.1016/j.ceramint. 2018.10.124

SOBRAL, J.M.; CARIDADE, S.G.; SOUSA, R.A.; MANO, J.F.; REIS, R.L.Three-dimensional plotted scaffolds with controlled pore size gradients: effect of scaffold geometry on mechanical performance and cell seeding efficiency, **Acta Biomater.** v.3, n.7, p. 1009-1018, 2011 doi.org/10.1016/j.actbio.2010.11.003.

TAO, Z. et al. Effects of strontium-modified calcium phosphate cement combined with bone morphogenetic protein-2 on osteoporotic bone defects healing in rats**. Journal of Biomaterials Applications,** [s. l.], v. 33, n. 1, p. 3–10, 2018.

THEIN-HAN, W.; XU, H.H. Prevascularization of a gas-foaming macroporous calcium phosphate cement scaffold via coculture of human umbilical vein endothelial cells and osteoblasts, **Tissue engineering**. Part A v.19, n.15-16, p.1675–1685, 2013.

TORRES, P.M.; GOUVEIA, S.; OLHERO, S.; KAUSHAL, A.; FERREIRA, J.M. Injectability of calcium phosphate pastes: Effects of particle size and state of aggregation of beta-tricalcium phosphate powders. **Acta Biomater.** v. 21, p. 204–216, 2015.

TOVANI, C.B.; OLIVEIRA, T.M.; SOARES, M.P.R. et al. Strontium Calcium Phosphate Nanotubes as Bioinspired Building Blocks for Bone Regeneration **ACS Appl. Mater.** Interfaces v.12, n.39, p. 43422−43434, 2020.

USKOKOVIC, V. Ion-doped hydroxyapatite: An impasse or the road to follow? **Ceram. Int**. v.46, p. 11443–11465, 2020.

WANG, L.; ZHANG, C.; LI, C.; WEIR, M.D.; WANG, P.; REYNOLDS, M.A.; ZHAO, L.; XU, H.H.K. Injectable calcium phosphate with hydrogel fibers encapsulating induced pluripotent, dental pulp and bone marrow stem cells for bone repair. **Materials Science and Engineering**. v.69, p. 1125-1136, 2016. https://doi.org/10.1016/j.msec.2016.08.019.

WEI, S.; MA, J.X.; XU, L. et al. Biodegradable materials for bone defect repair. **Military Medical Research** 2020 https://doi.org/10.1186/s40779-020-00280-6

ZHAO, L.; WEIR, M.D.; XU, H.H. An injectable calcium phosphate-alginate hydrogel-umbilical cord mesenchymal stem cell paste for bone tissue engineering. **Biomaterials.** v.31, n. 25, p. 6502-6510, 2010. doi:10.1016/j.biomaterials.2010.05.017

ZHANG, J.; LIU, W.; GAUTHIER, O. et al. A simple and effective approach to prepare injectable macroporous calcium phosphate cement for bone repair: Syringe-foaming using a viscous hydrophilic polymeric solution. **Acta Biomaterialia**. v.31, p.326-338, 2016. https://doi.org/10.1016/j.actbio.2015.11.055.

ZHANG, J.; LIU, W.; SCHNITZLER, V.; TANCRET, F.; BOULER, J-M.; Calcium phosphate cements for bone substitution: Chemistry, handling and mechanical properties **Acta Biomaterialia**. v.10, n.3, p.1035-1049, Mar. 2014. https://doi.org/ 10.1016/j. actbio.2013.11.001.

ZHONG, W.; SUN, L.; YU, T.; ZHOU, C. Preparation and characterization of calcium phosphate cement with enhanced tissue adhesion for bone defect repair **Ceram. Int.**, v.47, p. 1712-1720, 2021 10.1016/j.ceramint.2020.08.288

XIE, Y.; LIU, J.; BAO, X.; LI, Q.; XU, G. Setting Characteristics and High Compressive Strength of an Anti-washout, Injectable Calcium Phosphate Cement Combined with Thermosensitive Hydrogel. **Materials** v.13, p.5779, 2020 doi:10.3390/ma13245779